

1 **The Intra-Americas Sea: Challenges and Opportunities to Understand North**
2 **American Climate Variability and Predictability**

3
4 V. Misra^{1,2,3}, C. Wang⁴, Y. Serra⁵, K. Karnauskas⁶, E. M. Ellinor⁷, J. Sheinbaum⁸, P.
5 Chang^{9,10,11}, S. -K. Lee^{4,12}, B. Rosenheim¹³, B. Kirtman¹⁴, D. Enfield^{4,12}, E. D.
6 Maloney¹⁵, A. Kumar¹⁶, G. Poveda¹⁷, R. Fu¹⁸, J. Jouanno¹⁹, S. Berthet¹⁹, A. Mishra², M.
7 Bourassa^{1,2}, J. Candela⁸, and J. Ochoa⁸

8
9
10 1 Department of Earth, Ocean and Atmospheric Science, Florida State University

11 2 Center for Ocean-Atmospheric Prediction Studies, Florida State University

12 3 Florida Climate Institute, Florida State University

13 4 Atlantic Oceanographic and Meteorological Laboratory, NOAA, Miami FL

14 5 University of Arizona

15 6 Woods Hole Oceanographic Institution

16 7 School of Meteorology, The University of Oklahoma

17 8 Oceanografía Física, CICESE

18 9 Texas A&M University, Department of Oceanography, College Station, TX, US, 77843

19 10 Texas A&M University, Department of Atmospheric Sciences, College Station, TX,
20 US, 77843

21 11 Ocean University of China, Qingdao Collaborative Innovation Center of Marine
22 Science and Technology, Qingdao, China, 266100

23 12 Cooperative Institute for Marine and Atmospheric Studies, University of Miami,
24 Miami FL

25 13 College of Marine Science, University of South Florida

26 14 Rosenstiel School of Marine and Atmospheric Sciences, University of Miami

27 15 Department of Atmospheric Science, Colorado State University

28 16 Climate Prediction Center, National Centers for Environmental Prediction

29 17 Department of Geosciences and Environment, Universidad Nacional de Colombia,
30 Sede Medellin, Colombia

31 18 Department of Geological Sciences, Jackson School of Geosciences, The University
32 of Texas at Austin

33 19 Laboratoire d'Etudes en Géophysique et Oceanographie Spatiales

34

35
36
37
38
39
40
41
42
43
44
45
46
47
48
49
50
51
52
53
54

Abstract:

The Intra-Americas Seas (IAS), which includes the Gulf of Mexico and the Caribbean Sea, hosts part of the largest warm water pool in the Western Hemisphere and is a primary moisture source for precipitation in the Americas. This region undergoes significant variability from interannual to secular changes that impacts North American climate variability including the frequency of Atlantic tropical cyclones and southeast US tornadoes. Moisture evaporated from the IAS contributes to the severity of winter storms in the mid-Atlantic and northeast United States. The onset of North and South American monsoons also modify the trade winds with potential impacts on IAS surface fluxes and sea surface temperature (SST) variability. Most climate models display significant cold SST and dry rainfall bias over the IAS with a corresponding underestimation of their variability. In addition significant biases in IAS surface and deep ocean currents, and poor representation of the atmospheric low-level jets in the region are also apparent in the many of the climate models. Lack of observations in both the atmosphere and ocean in the IAS, which is one of the most poorly observed regions of the world, limits our ability to improve models. This paper provides recommendations to advance understanding of IAS climate variability and improve its predictability in the midst of a rapid deterioration of the observing network across the region.

55 **1 Introduction**

56 The Western Hemisphere Warm Pool (WHWP) located between North and South
57 America and between the tropical North Pacific and Atlantic Ocean (Fig. 1a) is the
58 second largest body of very warm water ($\geq 28.5^\circ\text{C}$) on Earth and hosts the second largest
59 diabatic heating center of the tropics during the boreal summer (Wang and Enfield 2001).
60 The WHWP spans the northeast tropical Pacific west of Central America (also known as
61 the Eastern Pacific Warm pool [EPWP]), the Intra-Americas Sea (IAS; i.e., the Gulf of
62 Mexico and the Caribbean Sea) and the western tropical North Atlantic (the latter two
63 regions also collectively referred to as the Atlantic Warm Pool [AWP]; Wang and Enfield
64 2001, 2003). The AWP serves as a host to nearly 80% of the WHWP and dominates the
65 variability of the latter. The WHWP appears first in late boreal spring in the northeast
66 Pacific followed by a warming in the Atlantic in boreal summer and fall. As a
67 consequence of its geographic location and strong sea surface temperature (SST)
68 variations superposed on a warm ocean basic state, the IAS plays a significant role in
69 modulating atmospheric and terrestrial variability both locally within the IAS and over
70 North America, particularly over the continental United States [CONUS], Central
71 America and northern South America (Wang et al. 2006, 2008; Ruiz-Barradas and Nigam
72 2005; Mestas-Nunez et al. 2007; Misra et al. 2014; Poveda et al. 2014).

73 The IAS is a complex system influenced by large-scale atmospheric features
74 including the North Atlantic Subtropical High (NASH), the monsoon systems of the
75 Americas, and the (continental and oceanic) Inter-Tropical Convergence Zones (ITCZs).
76 Seasonally persistent small-scale features such as atmospheric low level jets (LLJs; e.g.
77 North American, Choco, Tehuantepec, Papagayo LLJs) arising from the complex

78 topography (Fig. 1b) and seasonal migration of the NASH are also important in the
79 region. Ocean processes impacting the region include the upper branch of the Atlantic
80 Meridional Overturning Circulation (AMOC) that includes the Loop Current and the
81 associated eddies in the Gulf of Mexico (GoM), prevalent subtropical cells, and the
82 Caribbean current system with its ubiquitous mesoscale and sub-mesoscale eddies
83 sustained by a complex bathymetry (Fig. 1b). Embedded within these defining features of
84 the IAS are extreme events such as Atlantic, GoM, and Caribbean tropical cyclones
85 (TCs), tornadoes in the CONUS, monsoon severe thunderstorms, large and intense meso-
86 scale convective systems over the far eastern tropical Pacific and climate anomalies that
87 arise largely in response to variability on time scales ranging from intraseasonal to
88 secular changes in the IAS (Maloney and Hartmann 2000a, b; Wang and Lee 2007; Wang
89 et al. 2007, 2008a; Klotzbach 2014; Crosbie and Serra 2014; Serra et al. 2014). The
90 purpose of this paper is to highlight IAS variability and its role in regulating the climate
91 of North America, followed by a discussion of the limitations of our current climate
92 models and observational networks to effectively predict and monitor the observed IAS
93 climate, respectively. We present recommendations and emerging opportunities to
94 improve climate predictability and monitoring of IAS variability spanning from intra-
95 seasonal timescales to secular changes.

96

97 **2 The IAS Teleconnections**

98 The WHWP that includes the AWP defined by the 28.5°C surface isotherm (Fig.
99 1a) has a distinct seasonal cycle (Wang and Enfield 2001, 2003; Enfield and Lee 2005;

100 Lee et al. 2007) with a maximum around September 3 (Misra et al. 2014). The choice of
101 the 28.5°C isotherm to define the AWP stems from its close correspondence with the
102 variations in the IAS mixed layer depth (Wang and Enfield 2003), its notable impact on
103 organized convection (Graham and Barnett 1987), and the display of the strongest
104 interannual variations of the area enclosed by this isotherm in the IAS (Misra et al. 2013).
105 The variability of the WHWP is dominated by the AWP variability owing to its relative
106 size and seasonal persistence compared to the EPWP component (Wang et al. 2008a).
107 However the EPWP plays an important role in the North American Monsoon (NAM)
108 variability (Adams and Comrie 1997) and also serves as a precursor to the development
109 of the AWP (Enfield and Lee 2005; Lee et al. 2007).

110 The AWP-induced diabatic heating at its seasonal peak forces a Gill-type
111 atmospheric response as well as extratropical stationary waves (Fig. 2) that produces
112 rainfall variability over the CONUS (Fig. 3a), while modulating the subtropical highs in
113 the southeastern Pacific and in the North Atlantic Oceans (Fig. 3b). AWP variations and
114 their teleconnections to North American hydroclimate are also observed to be largely
115 independent of the El Niño and the Southern Oscillation (ENSO) variations in the
116 equatorial Pacific (Wang et al. 2006, 2008; Misra et al. 2013).

117 During the boreal summer season, easterly trade winds carry moisture from the
118 Tropical North Atlantic (TNA) into the Caribbean Sea where the flow intensifies forming
119 the easterly Caribbean low-level jet (CLLJ) due to a strong meridional pressure gradient
120 established by the NASH (Fig. 1a; Amador and Magana 1999; Poveda and Mesa 1999;
121 Wang 2007). As the CLLJ transits the Caribbean Sea, it splits into two branches: one
122 turning northward and forming the Great Plains LLJ (GPLLJ) while the other branch

123 continues westward across Central America into the eastern North Pacific (Fig. 1a).
124 Modeling and observational studies indicate that a large (small) AWP is associated with
125 weakening (strengthening) of the summertime NASH and strengthening (weakening) of
126 the summertime continental low over the NAM region (Fig. 3b; Wang et al. 2008a). The
127 observational studies also confirm that in response to the pressure changes, a large
128 (small) AWP weakens (strengthens) the southerly GPLLJ (e.g. Wang 2007), which
129 results in reduced (enhanced) northward moisture transport from the GoM to the region
130 east of the Rocky Mountains and thus decreases (increases) the moisture available for
131 summer rainfall over the central United States (Wang et al. 2006; Ruiz-Barradas and
132 Nigam 2006; Mestas-Nuñez et al. 2007).

133 An anomalously strong CLLJ is also associated with reduced precipitation over the
134 Caribbean and northern South America, including portions of Colombia and Venezuela
135 (Fig. 3; Poveda and Mesa, 1999; Wang 2007; Cook and Vizy 2010; Martin and
136 Schumacher, 2011b) and along the Pacific coast of Central America (Amador 1998).
137 Concomitantly, a strong CLLJ is associated with above normal rainfall over the
138 Caribbean coast of Central America, including Nicaragua and Costa Rica, particularly
139 during the boreal summer (May–September), through orographic enhancement and large-
140 scale low-level convergence at the jet exit (Waylen et al. 1996; Magaña et al., 1999;
141 Amador et al. 2000; Magaña and Caetano, 2005). Such enhanced summertime convective
142 activity on the upslope side of the terrain acts to deprive moisture to the Pacific coast of
143 Central America and results in rainfall deficits there (Amador 1998; Cook and Vizy
144 2010; Martin and Schumacher 2011b).

145 The rainfall over the AWP alternates with the Amazon basin in South America as
146 the seasonal heating source for the regional Hadley and Walker type circulations in the
147 Western Hemisphere (Wang et al. 2006; Poveda et al. 2006). During the boreal
148 summer/fall season, a strong regional Hadley-type circulation is established, with
149 ascending motion over the AWP and subsidence over the southeastern tropical Pacific. A
150 large (small) AWP during the boreal summer/fall results in a strengthening (weakening)
151 of this regional Hadley-type circulation with enhanced descent (ascent) over the
152 southeastern tropical Pacific (Wang et al. 2006, 2010, 2014; Lee et al. 2013b).

153

154 **3 Secular change in the IAS**

155 Among the challenges in interpreting observations of climate variability in the
156 IAS region are the detection and attribution of low–frequency variability and long–term
157 trends in SST. In particular, the IAS region is home to substantial internal multidecadal
158 variability (Ting *et al.* 2011) that can mask forced long–term trends using instrumental
159 records alone (Wang and Dong 2010) and often require historical hindcast model
160 experiments to interpret (Ting *et al.* 2009). Moreover, future hydroclimate projections by
161 state–of–the–art GCMs suggest that part of the IAS region including EPWP eastward
162 through the Caribbean islands (including Central America, Mexico, and the southern
163 United States) should anticipate a robust and severe reduction in precipitation (Neelin *et*
164 *al.* 2006; Meehl *et al.* 2007; Taylor *et al.* 2012; Maloney *et al.* 2014), which is thought to
165 be critically dependent on the magnitude and spatial patterns of ocean warming (Schubert
166 *et al.* 2009; Xie *et al.* 2010; Rauscher *et al.* 2011; Lee et al. 2011).

167 Future projections by the Coupled Model Intercomparison Project phase 5
168 (CMIP5) models predict that under the Representative Concentration Pathway (RCP8.5),
169 GoM SST will warm in a spatially uniform fashion in the multi-model ensemble mean at
170 a rate of 3–4°C century⁻¹ by the end of the 21st century, and 2–3°C century⁻¹ in the
171 Caribbean Sea (IPCC AR5, WG1, Ch. 12, Fig. 12.11 [Collins *et al.* 2013]). The projected
172 trends in these marginal seas approximately mirror those for the open Atlantic Ocean
173 regions immediately to their east.

174 A comparison of four gridded instrumental datasets (see supplementary material
175 [SM] S.1) agree on a broad warming across the western Tropical Atlantic Ocean and the
176 Caribbean Sea of ~0.4°C century⁻¹ with the greatest warming found along the northern
177 coast of South America in the southern Caribbean Sea (Fig. SF1). In stark contrast, SST
178 trends within the GoM are spatially heterogeneous and vary substantially from one
179 gridded product to another (Fig. SF1). Of particular relevance to recent and ongoing
180 observational efforts is that SST changes in the GoM are highly divergent among the four
181 data sets, varying by ~0.5°C relative to their 1951-1980 base periods. Published proxy
182 reconstructions of water temperature corroborate the trends in the super ensemble of
183 observations¹ (Fig. 4). The strongest proxy reconstruction trends are in the central
184 Caribbean Sea (Fig. 4), where the super ensemble shows agreement with a positive trend.
185 The weakest trends are in the GoM, but they are calculated from sediment cores with few
186 points covering the 20th century (Richey *et al.*, 2004; Richey *et al.*, 2008). The record
187 from the Cariaco Basin (off the north central coast of Venezuela; Black *et al.*, 2008) is
188 based on high time resolution through the 20th century, and it is the only proxy

¹ See SM S.1 on further details of super ensemble of observations

189 reconstruction in the basin that approaches the sign and magnitude of the trends in the
190 super ensemble. The magnitude of these trends are based on species-specific calibrations
191 that, in the case of the Caribbean Sea and GoM, seem to over-estimate long-term
192 temperature change. It is important to note that records from Jamaica (Hase-Schramm et
193 al., 2003), Pedro Bank (central Caribbean, Haase-Schramm et al., 2003), and the
194 Bahamas (Rosenheim et al., 2005) are from shallow subsurface records (28–67m). The
195 general pattern of change in the instrumental SST products (smaller and/or less robust
196 warming trends in the GoM than in the Caribbean Sea) is exactly opposite to the future
197 trends projected by CMIP5 models.

198 It is important to point however that future projections by CMIP5 models may
199 need to be downscaled to better understand the regional response of the IAS as they seem
200 to have significant ocean circulation bias in the IAS (Liu et al. 2102, 2015). Liu et al.
201 (2015) downscaled the CMIP5 model simulations under historical and two future
202 emission scenarios using an eddy-resolving regional ocean model. They reported that the
203 simulated volume transport by the western boundary current system in the IAS, including
204 the Caribbean, Yucatan and Loop Currents, was reduced by 20-25% during the 21st
205 century, consistent with a similar rate of reduction in the AMOC. Their modeling
206 analysis also showed that the projected reduction of the IAS western boundary current
207 system was linked to reduced upwelling and enhanced warming along the western
208 boundary.

209

210 **4 The monsoons and the IAS**

211 The IAS by its proximate location to the monsoons of the Americas serves as a
212 bridge to unify the South American Monsoon (SAM) and North American Monsoon
213 (NAM) systems. Observations have shown an anti-correlation between boreal winter
214 rainfall anomalies over the IAS region and those over the NAM and Southern Amazonia
215 on interannual (Wang and Fu 2002) and multi-decadal scales (Arias et al. 2014). On
216 interannual time scales these relationships are linked by the reversal of the cross-
217 equatorial flow over the Americas associated with ENSO (Arias et al. 2014). Misra and
218 DiNapoli (2013) also find that the anomalous meridional migration of the ITCZ in the
219 western Atlantic Ocean dictated by the intensity of the seasonal rainfall activity in the
220 equatorial Amazon during boreal winter is associated with the upper ocean heat content
221 and surface temperature variability of the IAS in the subsequent seasons (Fig. 5). This
222 teleconnection is established by the modulation of the atmospheric heat fluxes regulated
223 by the overlying regional Hadley circulation, which gives rise to a robust negative
224 correlation between austral summer rainfall over the equatorial Amazon and SST
225 variability in the IAS during the subsequent boreal summer season.

226 On decadal time scales the anti-correlation of rainfall between the NAM and the
227 SAM is also related to the intensification of rainfall over the IAS region, causing an early
228 retreat of the NAM and a late onset of the rainy season over southern Amazonia. These
229 variations seem to be a combined result of the westward shift of the NASH and the warm
230 phase of the Atlantic Multidecadal Oscillation (AMO; Arias et al. 2014).

231 Previous studies on the sources of NAM moisture indicate that moisture at upper
232 levels (above 700 hPa) originates to the east of the Sierra Madres Occidental and over the
233 GoM, while low-level moisture of oceanic sources originates predominantly from the

234 tropical Pacific Ocean and the Gulf of California (Schmitz and Mullen 1996; Adams and
235 Comrie 1997). In addition to these oceanic sources, studies using a two-dimensional
236 dynamic recycling model find that NAM terrestrial evapotranspiration accounts for
237 approximately 40% of the total moisture sources to the NAM (Dominguez et al. 2006; Hu
238 et al. 2014), similar to estimates of terrestrial sources for the May-July period based on
239 moisture tracers in a GCM (Bosilovich 2003).

240 While the seasonal migration of the monsoon ridge is fundamental to the onset
241 and demise of the NAM, monsoon precipitation is highly dependent upon intra-seasonal
242 variability (ISV), especially in the southwestern United States at the northern edge of the
243 monsoon. ISV in the IAS (see Serra et al. 2014 for a review) plays a particularly
244 important role in supporting NAM rainfall events through gulf surges, or surges of
245 moisture up the Gulf of California (e.g., Stensrud et al. 1997), and through IAS TC
246 activity that recurves directly over the NAM region (Collins and Mason 2012; Ritchie et
247 al. 2011; Corbosiero et al. 2009; Wood and Ritchie 2013). The link between tropical
248 disturbances, gulf surges, the MJO, and NAM rainfall events has not been fully explored;
249 however studies suggest that positive rainfall anomalies extend into the NAM region
250 during the transition to the MJO westerly phase, when TC and easterly wave activity is
251 also enhanced and shifted along the Mexican west coast (Lorenz and Hartmann 2006;
252 Crosbie and Serra 2014; see SM [S.2])

253 The Mid-Summer Drought (MSD; Fig. 6) phenomenon characterized by a
254 minimum in rainfall that separates two peaks in rainfall across the Caribbean and Central
255 America during boreal summer season has been associated with the westward expansion
256 and intensification of the NASH and associated CLLJ variability resulting in moisture

257 flux divergence (Hastenrath 1976, 1978; Granger 1985; Magana et al. 1999; Giannini et
258 al. 2000; Mapes et al. 2005; Wang 2007; Wang and Lee 2007; Misra et al. 2014). As the
259 NASH expands westward during the summer months precipitation is suppressed via
260 large-scale subsidence and increased stability (Knaff, 1997; Mapes et al. 2005; Wang and
261 Lee 2007; Kelly and Mapes 2011). In addition, the enhancement of the easterly trade
262 winds in the CLLJ leads to greater evaporative cooling and lower SSTs which further
263 suppresses convection (Muñoz et al. 2008, Xie 2006, Martin and Schumacher 2011b).

264

265 **5 The ocean circulation in the IAS**

266 The IAS is comprised of a very complex ocean circulation system from the
267 smallest spatial scales (e.g. ubiquitous presence of mesoscale and sub-mesoscale eddies;
268 see SM [S.3]) to hosting the upper branch of the AMOC (e.g. Caribbean current system,
269 GoM loop current and the southern branch of the Gulf stream system). These ocean
270 current systems that bring relatively warm and saline water from the equatorial Atlantic
271 to the GoM are fundamental to the regulation of the SST in the IAS (Jayne and Maotzke
272 2002; Chang and Oey 2010; Liu et al. 2012; Misra et al. 2015). Owing primarily to
273 shortcomings in long-term observational network of the IAS, substantial uncertainty
274 exists regarding the magnitude of inter-annual flow variability within the channels
275 (Yucatan, Old Bahama [OBC] and Northwest Providence [NWP] channels) that connect
276 to the Florida Straits at 27° N (Rousset & Beal 2014; see SM [S.4]).

277 The southern Caribbean upwelling system significantly contributes to the mean
278 SST distribution and its seasonal and inter-annual variability in the Caribbean Sea. The
279 upwelling follows a semi-annual cycle resulting in surface manifestation of relatively

280 cold SST's, which peaks in December–March and July (Fig. 7) in response to semi-
281 annual intensification of the along-shore CLLJ (Wang 2007; Wang and Lee 2007) and its
282 associated changes in wind stress curl (Inoue et al. 2002; Andrade and Barton 2005;
283 Cook and Vizy 2010). Jouanno and Sheinbaum (2013) also find that vertical turbulent
284 mixing is important in regulating the surface cooling at the coast. The intense vertical
285 mixing at the coast arises from vertical shear between the shallow and strong Caribbean
286 Current and the subsurface Caribbean coastal undercurrent. This southern Caribbean
287 upwelling region limits the southward extent of the AWP during its onset and peak phase
288 (Lee et al. 2007) and modulates the meridional gradient of SST over the Venezuela and
289 Colombia basins, with possible feedback to the trade winds (Chang and Oey, 2013). See
290 SM (S.5) for further discussion on the rectification effect on the atmosphere from the
291 cold SST's of this upwelling region.

292 It is also observed that a net freshwater gain (loss) in the TNA region coincides
293 with the large (small) AWP regimes on multi-decadal timescales (Wang and Zhang 2013;
294 Zhang and Wang 2012). Zhang et al. (2014) further confirm that this AWP induced
295 freshwater flux plays a negative feedback role that acts to restore the AMOC from its
296 anomalous state through basin-scale gyre circulation adjustments.

297

298 **6 The IAS extremes**

299 A number of studies have shown that IAS variability modulates Atlantic TC activity
300 (Fig. 8; e.g. Molinari et al. 1997; Maloney and Hartmann 2000a,b; Higgins and Shi 2001;
301 Wang and Lee 2007, 2009; Wang et al. 2007, 2008a, 2011; Aiyyer and Molinari 2008;

302 Jiang et al. 2012; Klotzbach 2014; Crosbie and Serra 2014). Calculated over a 34-year
303 period (1979-2012), 90 named Atlantic TCs occurred in small AWP years versus 163 for
304 large AWP years (Fig. 8). Wang and Lee (2007) argued that the observed teleconnection
305 between IAS and Atlantic TC activity is a result of the IAS SST-forced changes of the
306 vertical wind shear and moist static stability in the Atlantic TC Main Development
307 Region (MDR). Several studies have also suggested an influence of the Atlantic
308 Meridional Mode (AMM) on the Atlantic TC activity (Vimont and Kossin 2007; Kossin
309 and Vimont 2007; Patricola et al. 2014).

310 Dynamically, the AWP-forced atmospheric circulation pattern is baroclinic within
311 the tropical latitudes, with a large warm pool producing a cyclone in the lower
312 troposphere and an anticyclone in the upper troposphere, both situated on the northern
313 flank of the AWP (Wang et al. 2008a; Fig. 2). This anomalous circulation structure
314 reduces the lower tropospheric easterly flow and the upper tropospheric westerly flow
315 over the AWP, thus reducing the vertical wind shear in a way that favors atmospheric
316 convection (or TC development; Wang et al. 2007; 2008a). Similarly, the modulation of
317 large-scale environmental factors including tropospheric humidity, vorticity, vertical
318 shear, and SST by the MJO and other modes of ISV can also manifest in IAS-Atlantic TC
319 and extreme rainfall teleconnections (Maloney and Hartmann 2000a; Camargo et al.
320 2009; Martin and Schumacher 2011a; Jiang et al. 2012). However, precursor disturbances
321 for TCs in the form of easterly waves are also modulated on intraseasonal timescales in
322 the IAS region (e.g. Maloney and Hartmann 2001; Crosbie and Serra 2014; Rydbeck et
323 al. 2014). Thermodynamically, the AWP increases convective available potential energy
324 (CAPE) that provides the fuel for moist convection and thus facilitates the formation and

325 development of TCs (Wang et al. 2008). AWP-forced extra-tropical stationary Rossby
326 waves influence the barotropic atmospheric flow over North America and the Atlantic
327 Ocean in boreal summer (Lee et al., 2009), which then affects the steering flow of North
328 Atlantic TCs (Wang et al., 2011; see SM [S.6]).

329 Boreal spring (April and May) is the primary season for tornadoes in the US. The
330 convergence of dry upper level air from higher latitudes and low-level warm moist air
331 from the GoM result in a conditionally unstable environment to the east of the Rockies
332 with a raised CAPE that make it conducive for tornadogenesis. Lee et al. (2013a) show
333 that the April-May tornado outbreaks in the US are significantly correlated with moisture
334 transport from the GoM (Fig. 9) and lower tropospheric vertical wind shear in the central
335 and eastern US. Muñoz and Enfield (2011) find that the tornadic activity in lower
336 Mississippi, Tennessee, and Ohio is particularly related to the interannual and decadal
337 variability of the LLJs (Caribbean and North American) that dictate the moisture flux to
338 the region.

339 The relatively warm SST in the GoM compared to surrounding areas can result in
340 rapid cyclogenesis in the boreal winter season. For example, the Superstorm of 1993 (12-
341 14 March) was comparable in strength to a category 1 hurricane, with winds reaching 70
342 kt along the storm path, and producing storm surges more than 10 ft along the northeast
343 Gulf Coast (Schumann et al. 1995; Bosart et al. 1996). The GoM is a well-known source
344 for winter cyclones (Dickinson et al. 1997). Among other atypical features of the
345 environment that led to the rapid cyclogenesis event of Superstorm of 1993 (see Bosart et
346 al. 1996), a well noted feature was the presence of Eddy Vasquez over the northwest
347 GoM (Fig. 10), a warm water eddy shed from the loop current (Schumann et al. 1995).

348 This warm eddy not only provided the necessary air-sea fluxes to rapidly develop the
349 extratropical cyclone but also provided a very strong surface temperature gradient
350 (baroclinicity) from the cold continental shelf waters (Schumann et al. 1995).

351

352 **7 The barrier layers of the IAS**

353 The thick and persistent barrier layers or fresh water lens that form in the
354 northwest tropical Atlantic Ocean is a result of the large volume of fresh water influx
355 from some of the major continental rivers in northern South America (e.g., Orinoco and
356 Amazon; Pailler et al., 1999). The barrier layers of the IAS are one of the most prominent
357 structures in the world tropical and subtropical oceans (Mignot et al. 2007), which reflect
358 the prevalence of the robust land-atmosphere-ocean coupling in the region. The mighty
359 Amazon and Orinoco River systems together form the biggest river system in the world
360 in terms of discharge (0.2 Sv). The Guyana current carries a significant portion of this
361 water into the Caribbean Sea during boreal summer and fall (Hu et al., 1997), providing
362 the largest term in the surface salinity balance of the region (Foltz and McPhaden, 2008;
363 see SM S.7).

364 Because of the barrier layer's role in trapping heat within the upper ocean layer
365 and reducing surface cooling, the barrier layer in the northwestern tropical Atlantic has
366 the potential to affect Atlantic TC activity (Ffield 2007; Vizy and Cook 2010, Balaguru et
367 al. 2012). When TCs pass over barrier layers, the reduced efficacy of vertical mixing in
368 these highly stratified layers leads to reduced SST cooling, which then impacts TC
369 evolution by maintaining strong air-sea fluxes. In the northwestern tropical Atlantic,

370 Balaguru et al (2012) reported that the mean intensification factor of Atlantic TCs
371 increases from 0.48 ms^{-1} over a 36-hour period in non-barrier layer regions to 0.98 ms^{-1}
372 in barrier layer regions.

373

374 **8 The limitations of numerical models simulating and predicting IAS climate**

375 The surface temperature of the IAS and its variability is grossly underestimated
376 by a majority of the CMIP models that participated in the IPCC AR4 and AR5 especially
377 in the boreal summer and fall seasons (Fig. 11; Misra et al. 2009; Kozar and Misra 2012;
378 Liu et al. 2012, 2013; Ryu and Hayhoe 2013). A majority of the CMIP5 models
379 underestimate the area of the AWP in their 20th century simulation (Fig. 11). Surface heat
380 budgets computed over the IAS reveal that the radiative fluxes of downwelling shortwave
381 and longwave radiation dominate the maintenance of the AWP (Misra et al. 2013).
382 However, the important and subtle role for air-sea turbulent fluxes in the variability of the
383 AWP and its interplay with the variability of the overlying low-level easterlies, which is
384 related to the strength and position of the NASH, cannot be overemphasized (Misra et al.
385 2009). Liu et al. (2012) and Misra et al. (2013) find that a majority of current Global
386 Circulation Models (GCMs) and reanalysis products of the ocean and the atmosphere
387 produce a qualitatively correct surface heat budget in the IAS. However, when compared
388 to reanalysis, GCMs have a tendency to underestimate latent heat flux and downwelling
389 shortwave flux, and overestimate sensible heat flux. Liu et al. (2012) also indicate that
390 the upper ocean heat budget in the GoM is a complex balance of contrasting warming
391 influence of upper ocean heat transports (e.g. Loop Current) and cooling influence of the

392 net surface flux. In effect with significant GCM biases prevalent in surface fluxes and
393 ocean circulation over the region (Liu et al. 2015), it is not surprising to note such large
394 SST errors over the IAS in GCMs (Fig. 11).

395 The GCMs also display severe bias over equatorial Atlantic. Like some of the
396 most fundamental features of the equatorial Atlantic Ocean – the east-west equatorial
397 SST gradient and the eastward shoaling thermocline – cannot be reproduced by most
398 global climate models (Fig. 12; e.g. Richter and Xie, 2008; Richter et al. 2014). It is
399 concerning that like the previous feature in Fig. 11, this grave bias in the equatorial
400 Atlantic has also persisted across generations of model development (Fig. 12). Xu et al.
401 (2014) found that the southeastern tropical Atlantic warm SST bias can remotely force a
402 significant cold SST bias and dry precipitation bias in the IAS region (see their Fig. 18).

403 The IAS region is characterized by significant deficiencies in the simulation of
404 convection and related processes. For example, ISV in the east Pacific and Caribbean is
405 overall poorly simulated in amplitude and spatial structure in climate models (Jiang et al.
406 2013), with poor performing models also tending to have common mean state biases in
407 winds and other fields. Martin and Schumacher (2012) and Ryu and Hayhoe (2013)
408 showed that cold SST bias of the IAS was the dominant cause of the negative rainfall bias
409 across CMIP3 coupled historical simulations. In more recent CMIP5 historical
410 simulations, large precipitation and SST biases across the Caribbean are still evident in
411 both coupled (historical) and uncoupled (AMIP) simulations (see SM [S.8]). CMIP5
412 models produce too little mean precipitation in Central America and adjacent regions of
413 the east Pacific and Caribbean during boreal summer in the multimodel mean, and also
414 not enough precipitation in Caribbean island regions (Sheffield et al. 2013). Furthermore,

415 the timing of NAM precipitation also exhibits substantial biases, with models generally
416 producing too little precipitation in the NAM region in early and mid boreal summer, and
417 excessive precipitation late in the monsoon period (Liang et al. 2008; Sheffield et al.
418 2014a), associated with difficulty in ending the monsoon (Geil et al. 2013).

419 Many of the biases described above may be related to deficiencies in the deep
420 convection parameterizations of climate models, and are further exacerbated by the large
421 SST bias in the IAS. For example, many deep convection parameterizations used in
422 climate models do not exhibit adequate sensitivity to free tropospheric humidity (e.g.
423 Derbyshire et al. 2004), or lack representations of cumulus momentum transport and the
424 effect of mesoscale circulations on convective gustiness that affects surface fluxes. Model
425 ISV in the IAS region can be improved by suppressing convection through enhanced
426 moisture sensitivity or other means, although often the quality of the mean state degrades
427 when such modifications are not done with care (e.g. Kim et al. 2011; Maloney et al.
428 2014a), suggesting that such changes can improve ISV for the wrong reasons (e.g.
429 Maloney et al. 2014a; Hannah and Maloney 2014).

430 The recent effort to make seasonal predictions from multiple models like the
431 North American Multi-Model Ensemble project (NMME; Kirtman et al. 2014) routinely
432 available allows us to assess skill of predicting SSTs over the AWP, and terrestrial
433 anomalies over the surrounding areas. Misra and Li (2014) find that the seasonal
434 predictability of the AWP in the NMME models is promising compared to earlier
435 generation GCMs (Misra et al. 2009), but also displays notable limitations. For example,
436 NMME mean forecasts indicate that skill in predicting seasonal mean SSTs in the AWP
437 is much less than the skill in predicting SST variability in the equatorial eastern Pacific

438 associated with ENSO (Fig. 13). Anomaly correlations averaged over the AWP region
439 are in the range of 0.5 – 0.6, much less compared to those over the eastern equatorial
440 Pacific (Niño3.4 region). Prediction of terrestrial climate anomalies around the IAS relies
441 on skillful prediction of IAS SSTs, and hence seasonal prediction over land areas cannot
442 be improved until skill in predicting SST is improved. An assessment of the
443 corresponding JJA seasonal mean precipitation anomalies confirms this (Fig. 14) in
444 which prediction skill (anomaly correlation of the ensemble mean) generally does not
445 exceed 0.3. See SM (S.10) for comparison of this skill with the boreal winter season.

446

447 **9 The observing network in the IAS**

448 A gradually and significantly degrading observational network for the atmosphere
449 and ocean in the IAS region also exacerbates the modeling challenges described in the
450 previous section. For example, the radiosonde network in the region is quite sparse (Fig.
451 SF10; SM [S.9]) and temporally incomplete. For a region that displays a highly
452 heterogeneous distribution of rainfall, the rain gauge network is highly inadequate (Fig.
453 SF11). The complex spatial structure of rainfall in the IAS (with topographic, island, and
454 LLJ effects) raises a challenge for observing and monitoring the climate of the region.
455 For example, Figs. 6a and b show rainfall measurements from the satellite based Tropical
456 Rainfall Measuring Mission (TRMM) and merged satellite and in-situ Global
457 Precipitation Climatology Project (GPCP) data, respectively, and differences between the
458 products are evident in both the location and magnitude of rainfall features across the
459 region. Using TRMM precipitation radar data, Sobel et al. (2011) show that rainfall

460 enhancement is more significant over larger (greater than 315 km²) islands than smaller
461 islands in the Caribbean and that smaller islands have a negligible or even negative
462 change in rainfall intensity and frequency relative to surrounding oceans. However, while
463 high-resolution satellite data such as TRMM and the newly launched Global Precipitation
464 Measurement (GPM) satellites can provide useful information, the 0.25° TRMM
465 resolution (~28km) provides fewer than 3 measurements for most of the smaller islands
466 in the Lesser Antilles. For example, the island of Dominica (approximately 25km wide
467 and 50 km long) has large meridional variations in rainfall intensity and frequency as
468 measured during the DOMEX (Dominica Experiment) field campaign that are not
469 captured by current satellite measurements of rainfall (Smith et al. 2012, Minder et al.
470 2013).

471 In-situ ocean observational networks in the IAS have also diminished
472 considerably over time. ARGO floats, which have the operating depth of about 2000m
473 cannot pass the Lesser Antilles to reach the Caribbean Sea. As a result, the IAS is
474 currently as poorly observed as the polar oceans (Fig. SF12). This poor observational
475 network leaves some basic issues unresolved including characteristics of the seasonal
476 cycle of the oceanic variables in the IAS and its relation to the Loop Current and eddy
477 shedding dynamics, and the different pathways of the flow that can impact the salt,
478 temperature and fresh water transport by the AMOC through the western boundary. As
479 mentioned earlier, there is significant disparity in the diagnosis of the observed long-term
480 variations of SST in the IAS.

481

482 **10 Discussion and Conclusions**

483 The IAS produces robust local and remote climate variability on intra-seasonal
484 timescales to decadal timescales, and also exhibits secular change. In the midst of weak
485 ENSO forcing over North America especially during boreal summer and fall seasons, the
486 the development of SST anomalies in the IAS region superimposed on a warm mean SST
487 state (WHWP) can influence atmospheric and terrestrial variability over remote regions
488 via different pathways, including modulation of low level moisture transport and changes
489 in convection over the AWP, including remote teleconnections induced by these
490 convection anomalies.

491 Coordinating with ongoing projects and leveraging technological advances could
492 significantly ameliorate the observational gaps in the IAS and its adjacent nations. For
493 example, in response to the need to monitor both short and long term natural hazards
494 throughout the Caribbean and Mexico, the National Science Foundation (NSF) has
495 funded two GPS-based atmospheric sounding initiatives: The Continuously Operating
496 Caribbean Observation Network (COCONet) (Braun et al. 2012) and the Trans-boundary,
497 Land and Atmosphere Long-term Observational and Collaborative Network
498 (TLALOCNet) in Mexico. Mexican partners, including the National Autonomous
499 University of Mexico (UNAM) will also add to this network (see SM S.11). Data
500 products from these networks include estimates of column integrated tropospheric water
501 vapor; surface meteorological variables including wind speed and direction, air
502 temperature, humidity and precipitation; time series of daily positions and component
503 velocities for each station (used to quantify tectonic changes in the region); and high-rate
504 low-latency data from a subset of stations. Similarly, new techniques like Global
505 Positioning System (GPS) Radio Occultation (RO) measurements can provide relatively

506 accurate atmospheric sounding data with high vertical resolution especially above the
507 atmospheric boundary layer (Anthes et al. 2008) that could supplement the sparse upper
508 air network in the region.

509 Several important measuring and modeling projects for the GoM are currently in
510 progress or are about to be financed either by the oil industry and/or government agencies
511 from different countries (e.g. the Gulf of Mexico Research Institute). A coordinated
512 approach to achieve some basic common goals among these projects could help sustain a
513 multinational long-term observing and monitoring program at least for the GoM. In
514 addition, new technologies including underwater gliders appear to be particularly ideal
515 for setting up a relatively low cost long-term observing program for the IAS in which
516 cross-sections across the Caribbean Current or in the Gulf of Mexico could be regularly
517 sampled. Choosing some of these sections to coincide with satellite-altimetry tracks
518 would provide invaluable information for calibration of altimetry against observed
519 stratification and heat content. Glider observations seem especially well suited for studies
520 of hurricane intensification, which could be supplemented with greater coverages by
521 surface drifters and IRIDIUM-controlled ARGO floats. A pilot underwater glider project
522 for the Caribbean Sea has already started since 2014
523 (<http://www.aoml.noaa.gov/phod/goos/gliders>). Coordinated intensive field observations
524 can also be planned to provide high temporal and spatial resolution atmospheric and
525 oceanic observations in limited regions to better understand local and regional physical
526 process and to provide high quality datasets for improving models. High resolution
527 modeling studies may also provide a bridge to improving global model physical
528 parameterizations, if coordinated with such field programs.

529 One of the current grand challenges in seasonal-to-interannual prediction is
530 rainfall during the warm season over North America, which is a difficult problem because
531 much of the rainfall is associated with relatively small-scale structures (e.g.,
532 thunderstorms and mesoscale convective complexes) that are not adequately resolved by
533 the current generation of seasonal-to-interannual prediction systems. As a consequence,
534 large systematic errors occur in the predicted rainfall anomalies that seriously limit
535 forecast quality. Fundamental predictability issues also exist, namely that remote forcing
536 from remote climate variability (e.g. ENSO) is relatively weak and the rainfall signal-to-
537 noise ratio over North America is comparatively small. Nevertheless, our current
538 understanding indicates that current prediction systems are underperforming, even with
539 the limited predictability (see SM [S.10]).

540 The IAS climate processes outlined in this paper provide opportunities to improve
541 local and remote North American hydroclimate prediction across temporal scales. An
542 opportunity also exists to provide a more holistic picture of Western Hemisphere climate
543 and its prediction by bridging tropical South American climate variability with that of the
544 IAS. Moving forward, the modeling and observational challenges of IAS have to be
545 overcome for improved climate monitoring and prediction to become reality for the ~600
546 million population of the IAS region.

547

548 **Acknowledgements**

549 We acknowledge the help of graduate student Michael Kozar of FSU in preparing Fig. 8.

550 We also thank Kevin O'Brien of NOAA for generating Fig. SF12. We also acknowledge

551 the support of NSF, NASA, NOAA, CISCE. We also acknowledge data resourced from
552 the NOAA/OAR/ESRL PSD, Boulder, Colorado, USA, from their Web site at
553 <http://www.esrl.noaa.gov/psd/>, UCAR from their website <http://dss.ucar.edu>

554

555 **References**

- 556 Adams, D. K., and A. C. Comrie, 1997: The North American Monsoon. *Bull. Amer.*
557 *Meteor. Soc.*, 78, 2197–2213.
- 558 Amador, J. A., 1998: climatic feature of the tropical Americas: The trade wind easterly
559 jet. *Top. Meteor. Oceanogr.* 5, 91–102.
- 560 Amador, J. A., and V. O. Magaña, 1999: Dynamics of the low level jet over the
561 Caribbean, in 23rd Conference on Hurricanes and Tropical Meteorology, pp. 868–
562 869, Am. Meteorol. Soc., Dallas, Texas.
- 563 Amador, J., Magaña, V., and Pérez, J., 2000: The low level jet and convective activity
564 in the Caribbean. In Preprints 24th Conf. in Hurricanes and Tropical Meteorology,
565 Fort Lauderdale, FL, AMS, pp. 114–115.
- 566 Andrade, C. A., and E. D. Barton, 2005: The Guajira upwelling system. *Cont. Shelf*
567 *Res.*, 25, 1003–1022.
- 568 Anthes, R. A., Y. H. Kuo, D. P. Baumhefner, R. P. Erico, and T. W. Bettge, 1985:
569 Predictability of mesoscale atmospheric motions. *Advances in Geophysics*, Vol.
570 28B, Academic Press, 159–202, doi:10.1016/S0065-2687(08)60188-0.
- 571 Aiyyer, A. and J. Molinari, 2008: MJO and Tropical Cyclogenesis in the Gulf of
572 Mexico and Eastern Pacific: Case Study and Idealized Numerical Modeling. *J.*
573 *Atmos. Sci.*, 65, 2691–2704.
- 574 Athie, G., Sheinbaum, J., Ochoa, J., Candela J., Leben, R. Interannual variability of the
575 flow at Yucatan Channel, submitted, *Geophysical research letters*, 2014.
- 576 Arias, P.A., R. Fu, and K. Mo, 2012: Changes in monsoon regime over northwestern
577 Mexico in recent decades and its potential causes. *J. Clim.*, 25, 4258–4274.
- 578 Black, D.E., Abahazi, M.A., Thunell, R.C., Kaplan, A., Tappa, E.J., Peterson, L.C.,
579 2007. An 8-century tropical Atlantic SST record from the Cariaco Basin:
580 Baseline variability, twentieth-century warming, and Atlantic hurricane
581 frequency. *Paleoceanography* 22, 10.
- 582 Bosart, L. F., G. J. Hakim, K. R. Tyle, M. A. Bedrick, M. J. Dickinson, and D. M.
583 Schultz, 1996: Large-scale antecedent conditions associated with the 12–14
584 March 1993 cyclone (“Superstorm ’93”) over eastern North America. *Mon.*
585 *Wea. Rev.*, 124, 1865–1891.
- 586 Bosilovich, M. G., 2003: Numerical simulation of the large-scale North American
587 monsoon water sources. *Journal of Geophysical Research Atmosphere*, 108, 8614,
588 doi:10.1029/2002JD003095.

- 589 Braun, J., and Coauthors, 2012: Focused Study of Interweaving Hazards Across the
590 Caribbean. *Eos, Trans. Amer. Geophys. Union*, 93, 89–90.
- 591 Breugem W.-P., P. Chang, C. J. Jang, J. Mignot and W. Hazeleger, 2008: Barrier layers
592 and tropical Atlantic SST biases in coupled GCMs, *Tellus A*, 60, 885–897,
593 DOI: 10.1111/j.1600-0870.2008.00343.x.
- 594 Camargo, S. J., M. C. Wheeler, and A. H. Sobel, 2009: Diagnosis of the MJO
595 Modulation of Tropical Cyclogenesis Using an Empirical Index. *J. Atmos. Sci.*,
596 66, 3061–3074.
- 597 Chang, Y. –L. and L. –Y. Oey, 2010: Eddy and wind forced heat transports in the Gulf
598 of Mexico. *J. Phys. Oceanogr.*, 40, 2727-2742.
- 599 Chang, Y-L., and L-Y. Oey, 2013: Coupled Response of the Trade Wind, SST
600 Gradient, and SST in the Caribbean Sea, and the Potential Impact on Loop
601 Current's Interannual Variability. *Journal of Physical Oceanography*, 43.7, 1325-
602 1344.
- 603 Chen, M., P. Xie, J. E. Janowiak, and P. A. Arkin, 2002: Global Land Precipitation: A
604 50-yr Monthly Analysis Based on Gauge Observations, *J. of Hydrometeorology*,
605 3, 249-266.
- 606 Cook, K. H., and E. K. Vizy (2010), Hydrodynamics of the Caribbean lowlevel jet and
607 its relationship to precipitation, *J. Clim.*, 23, 1477–1494.
- 608 Collins, M., R. Knutti, J. Arblaster, J.–L. Dufresne, T. Fichet, P. Friedlingstein, X.
609 Gao, W.J. Gutowski, T. Johns, G. Krinner, M. Shongwe, C. Tebaldi, A.J. Weaver
610 and M. Wehner, 2013: Long-term Climate Change: Projections, Com-
611 mitments and Irreversibility. In: *Climate Change 2013: The Physical Science*
612 *Basis. Contribution of Working Group I to the Fifth Assessment Report of the*
613 *Intergovernmental Panel on Climate Change* [Stocker, T.F., D. Qin, G.–K.
614 Plattner, M. Tignor, S.K. Allen, J. Boschung, A. Nauels, Y. Xia, V. Bex and P.M.
615 Midgley (eds.)]. Cambridge University Press, Cambridge, United Kingdom and
616 New York, NY, USA.
- 617 Crosbie, E., and Y. Serra, 2014: Intra-seasonal Modulation of Synoptic Scale
618 Disturbances and Tropical Cyclone Genesis in the Eastern North Pacific. *J.*
619 *Climate*, in press.
- 620 Dickinson, M. J., and coauthors, 1997: The March 1993 superstorm cyclongenesis:
621 Incipient phase synoptic and convective scale flow interaction and model
622 performance. *Mon. Wea. Rev.*, 125, 3041-3072.
- 623 Dominguez, F., P. Kumar, X.-Z. Liang, and M. Ting, 2006: Impact of Atmospheric
624 Moisture Storage on Precipitation Recycling. *Journal of Climate*, 19, 1513–1530,
625 doi:10.1175/JCLI3691.1.

- 626 Feng, S., Q. Hu, and R. J. Oglesby, Influence of Atlantic sea surface temperatures on
627 persistent drought in North America, *Clim. Dyn.*, 37, 569–586,
628 doi:10.1007/s00382-010-0835-x, 2011.
- 629 Ffield, A., 2007: Amazon and Orinoco River Plumes and NBC Rings: Bystanders or
630 Participants in Hurricane Events? *J. Climate*, 20, 316–333. doi:
631 <http://dx.doi.org/10.1175/JCLI3985.1> .
632
- 633 Foltz, G.R. and M.J. McPhaden, 2009: Impact of barrier layer thickness on SST in the
634 central tropical North Atlantic, *J. Climate*, 22, 285–299.
- 635 Geil, K. L., Y. L. Serra, and X. Zeng, 2013: Assessment of CMIP5 model simulations
636 of the North American monsoon system. *J. Climate*, 26, 8787–8801.
- 637 Giannini, A., Y. Kushnir, and M. A. Cane, 2000: Interannual variability of Caribbean
638 rainfall, ENSO, and the Atlantic Ocean, *J. Climate*, 13, 297–311.
- 639 Graham, N. E., and T. P. Barnett, 1987: Sea surface temperature, surface wind
640 divergence, and convection over tropical oceans. *Science*, 238, 657–659.
- 641 Granger, O. E., 1985: Caribbean climates, *Prog. Phys. Geogr.*, 9, 16–43.
- 642 Haase-Schramm, A., Böhm, F., Eisenhauer, A., Dullo, W.-C., Joachimski, M.M.,
643 Hansen, B., Reitner, J., 2003. Sr/Ca ratios and oxygen isotopes from
644 sclerosponges: temperature history of the Caribbean mixed layer and thermocline
645 during the Little Ice Age. *Paleoceanography* 18, doi: 10.1029/2002PA00008
- 646 Hannah, W. M., and E. D. Maloney, 2014: The Moist Static Energy Budget in NCAR
647 CAM5 Hindcasts during DYNAMO. *J. Adv. Modeling Earth Sys.*, 6,
648 doi:10.1002/2013MS000272.
- 649 Hartmann, D. L., and E. D. Maloney, 2001: The Madden-Julian oscillation, barotropic
650 dynamics, and north Pacific tropical cyclone formation. Part II: Stochastic
651 barotropic modeling. *J. Atmos. Sci.*, 58, 2559–2570.
- 652 Hastenrath, S., 1976: Variations in low-latitude circulation and extreme climatic events
653 in the tropical Americas, *J. Atmos. Sci.*, 33, 202–215.
- 654 Hastenrath, S., 1978: On modes of tropical circulation and climatic anomaly, *J. Atmos.*
655 *Sci.*, 35, 2222–2231.
- 656 Hetzinger, S., Pfeiffer, M., Dullo, W.C., Garbe-Schonberg, D., Halfar, J., 2010. Rapid
657 20th century warming in the Caribbean and impact of remote forcing on climate
658 in the northern tropical Atlantic as recorded in a Guadeloupe coral. *Paleogeogr.*
659 *Paleoclimatol. Paleoecol.* 296, 111–124.

- 660 Higgins, R. W., W. Shi, 2001: Intercomparison of the Principal Modes of Interannual
661 and Intraseasonal Variability of the North American Monsoon System. *J. Climate*,
662 14, 403–417.
- 663 Hirahara, S., M. Ishii, and Y. Fukuda, 2014: Centennial–Scale Sea Surface
664 Temperature Analysis and Its Uncertainty. *J. Climate*, **27**, 57–75.
- 665 Hu, C. et al., The dispersal of the Amazon and Orinoco river water in the tropical
666 Atlantic and Caribbean sea : Observation from space and S-PALACE floats,
667 Deep-sea research II, 51, 2004.
- 668 Huancui Hu and Francina Dominguez, 2014: Evaluation of Oceanic and Terrestrial
669 sources of moisture for the North American Monsoon using Numerical Models
670 and Precipitation Stable Isotopes. *J. Hydrometeorology*, submitted
- 671 Inoue, M., I. C. Handoh, and G. R. Bigg, 2002: Bimodal distribution of tropical
672 cyclogenesis in the Caribbean: Characteristics and environmental factors. *J.*
673 *Climate*, 15, 2897–2905.
- 674 Jayne, S. R. and J. Marotzke, 2002: The oceanic eddy heat transport. *J. Phys.*
675 *Oceanography*, 32, 3328-3345.
- 676 Jiang, X., and D. E. Waliser, 2009: Two dominant subseasonal variability modes of the
677 eastern Pacific ITCZ, *Geophys. Res. Lett.*, 36, L04704,
- 678 Jiang, X., M. Zhao, and D. E. Waliser, 2012: Modulation of tropical cyclone activity by
679 the tropical intraseasonal oscillation over the Eastern Pacific in a high resolution
680 GCM, *Journal of Climate*, 25, 6524-6538.
- 681 Jiang, X.-A., E. D. Maloney, J.-L. F. Li, and D. E. Waliser, 2013: Simulations of the
682 eastern north Pacific intraseasonal variability in CMIP5 GCMs. *J. Climate*, 26,
683 3489-3510.
- 684 Jouanno, J., J. Sheinbaum, B. Barnier, J.-M. Molines, and J. Candela, 2012: Seasonal
685 and interannual modulation of the eddy kinetic energy in the Caribbean Sea. *J.*
686 *Phys. Oceanogr.*, 42, 2041–2055.
- 687 Jouanno, J. and J. Sheinbaum, 2013: Heat Balance and Eddies in the Caribbean
688 Upwelling System . *J. Phys. Oceanogr.*, 43, 1004-1014, DOI: 10.1175/JPO-D-12-
689 0140.1 .
- 690 Kaplan, A., M. Cane, Y. Kushnir, A. Clement, M. Blumenthal, and B. Rajagopalan,
691 1998: Analyses of global sea surface temperature 1856–1991. *J. Geophys. Res.*,
692 **103**, 18 567–18 589.
- 693 Kelly P and Mapes B (2011) Zonal mean wind, the Indian monsoon, and July drying in
694 the western Atlantic subtropics. *J. Geophys. Res.* 116:D00Q07.
695 doi:10.1029/2010JD015405.

- 696 Kilbourne, K.H., Quinn, T.M., Guilderson, T.P., Webb, R.S., Taylor, F.W., 2007.
697 Decadal- to interannual-scale source water variations in the Caribbean Sea
698 recorded by Puerto Rican coral radiocarbon. *Climate Dynamics* 29, 51-62.
- 699 Kim, D., A. H. Sobel, E. D. Maloney, D. M. W. Frierson, and I.-S. Kang, 2011: A
700 systematic relationship between intraseasonal variability and mean state bias. *J.*
701 *Climate*, 24, 5506-5520.
- 702 Kirtman, B. P., et al. (2014), The North American Multi-1 Model Ensemble (NMME):
703 Phase-1 Seasonal to Interannual Prediction, Phase-2 Toward Developing Intra-
704 Seasonal Prediction, *Bull. Am. Meteorol. Soc.*, doi:10.1175/BAMS-D-12-00050.1
- 705 Kossin, J. P., and D. J. Vimont, 2007: A more general framework for understanding
706 Atlantic hurricane variability and trends. *Bull. Amer. Meteor. Soc.*, 88, 1767-
707 1781.
- 708 Kozar, M. and V. Misra, 2012: Evaluation of twentieth-century Atlantic Warm Pool
709 simulations in historical CMIP5 runs *Clim. Dyn.*, 41(9-10), 2375-2391,
710 doi:10.1007/s00382-012-1604-9.
- 711 Klotzbach, P. J., 2014: The Madden–Julian Oscillation’s Impacts on Worldwide
712 Tropical Cyclone Activity. *J. Climate*, 27, 2317–2330.
- 713 Knaff, J. A., 1997: Implications of summertime sea level pressure anomalies in the
714 tropical Atlantic region, *J. Climate*, 10, 789–804.
- 715 Kushnir, Y., R. Seager, M. Ting, N. Naik, and J. Nakamura, Mechanisms of tropical
716 Atlantic SST influence on north american precipitation variability, *Journal of*
717 *Climate*, 23, doi:10.1175/2010JCLI3172.1, 2010.
- 718 Lee, S.-K., D. B. Enfield, and C. Wang. What Drives Seasonal Onset and Decay of the
719 Western Hemisphere Warm Pool? 2007: *J. Clim.*, 20, 2133-2146
- 720 Lee, S.-K., C. Wang, and B.E. Mapes, 2009: A simple atmospheric model of the local
721 and teleconnection responses to tropical heating anomalies. *Journal of Climate*,
722 22(2):227-284.
- 723 Lee, S.-K., D. B. Enfield and C. Wang, 2011: Future impact of differential inter-basin
724 ocean warming on Atlantic hurricanes. *J. Climate*, 24, 1264-1275.
- 725 Lee S.-K., R. Atlas, D.B. Enfield, C. Wang and H. Liu, 2013a. Is There An Optimal
726 ENSO Pattern That Enhances Large-scale Atmospheric Processes Conducive to
727 Major Tornado Outbreaks in the U.S.? *Journal of Climate*, 26(5):1626-1642,
728 doi:10.1175/JCLI-D-12-00128.1.
- 729 Lee, S.-K., C. R. Mechoso, C. Wang and J. D. Neelin, 2013b: Interhemispheric
730 influence of the northern summer monsoons on the southern subtropical

- 731 anticyclones. *J. Climate*, 26, 10193-10204. doi:[http://dx.doi.org/10.1175/JCLI-D-](http://dx.doi.org/10.1175/JCLI-D-13-00106.1)
732 13-00106.1.
- 733 Liang, X.-Z., J. Zhu, K. E. Kunkel, M. Ting, and J. X. L. Wang, 2008: Do CGCMs
734 simulate the North American monsoon precipitation seasonal–interannual
735 variations? *J. Climate*, 21, 3755–3775.
- 736 Liu, H., C. Wang, S.-K. Lee, and D. B. Enfield, 2013: Atlantic warm pool variability in
737 the CMIP5 simulations. *Journal of Climate*, 26: 5315-5336.
- 738 Liu, H., C. Wang, S.-K. Lee, and D.B. Enfield, 2012: Atlantic warm pool variability in
739 the IPCC-AR4 CGCM simulations. *Journal of Climate*, 25:5612-5628.
- 740 Liu, Y., S.-K. Lee, B. A. Muhliling, J. T. Lamkin and D.B. Enfield, 2012: Significant
741 reduction of the Loop Current in the 21st century and its impact on the Gulf of
742 Mexico. *J. Geophys. Res.*, 117, C05039, doi:10.1029/2011JC007555.
- 743 Liu, Y., S.-K. Lee, D. B. Enfield, B. A. Muhliling, J. T. Lamkin, F. Muller-Karger and
744 M. A. Roffer, 2015: Potential impact of climate change on the Intra-Americas
745 Seas: Part-1. A dynamic downscaling of the CMIP5 model projections. *J. Marine*
746 *Syst.*, 148, 56-69, doi:10.1016/j.jmarsys.2015.01.007.
- 747 Magaña V., J. A. Amador and S. Medina, 1999: The midsummer drought over Mexico
748 and Central America. *J. Climate* 12, 1577-1588.
- 749 Magaña, V., and Caetano, E., 2005: Temporal evolution of summer convective activity
750 over the Americas warm pools. *Geophys. Res. Lett.*, 32,
751 doi:10.1029/2004GL021033.
- 752 Maloney, E. D., and D. L. Hartmann, 2000a: Modulation of hurricane activity in the
753 Gulf of Mexico by the Madden-Julian oscillation. *Science*, 287, 2002-2004.
- 754 Maloney, E. D., and D. L. Hartmann, 2000b: Modulation of eastern north Pacific
755 hurricanes by the Madden-Julian oscillation. *J. Climate*, 13, 1451-1460.
- 756 Maloney, E. D., and D. L. Hartmann, 2001: The Madden-Julian oscillation, barotropic
757 dynamics, and north Pacific tropical cyclone formation. Part I: Observations. *J.*
758 *Atmos. Sci.*, 58, 2545-2558.
- 759 Maloney, E. D., and S. K. Esbensen, 2003: The amplification of east Pacific Madden-
760 Julian oscillation convection and wind anomalies during June-November. *J.*
761 *Climate*, 16, 3482-3497.
- 762 Maloney, E. D., X. Jiang, S.-P. Xie, and J. J. Benedict, 2014a: Process-oriented
763 diagnosis of east Pacific warm pool intraseasonal variability. *J. Climate*, 27, 6305-
764 6324.

- 765 Mapes, B. E., P. Liu, and N. Buening, 2005: Indian monsoon onset and the Americas
766 midsummer drought: Out-of equilibrium response to smooth seasonal forcing. *J.*
767 *Climate*, 18, 1109–1115.
- 768 Martin, E.R., and C. Schumacher, 2011a,: Modulation of Caribbean precipitation by the
769 Madden–Julian oscillation. *J. Climate*, 24, 813–824
- 770 Martin, E. R., and C. Schumacher, 2011b. The Caribbean low-level jet and its
771 relationship with precipitation in IPCC AR4 models. *J. Climate*, 24, 5935–5950.
- 772 Martin, E. R., and C. Schumacher, 2012. The relationship between tropical warm pool
773 precipitation, sea surface temperature, and large-scale vertical motion in IPCC
774 AR4 models. *J. Atmos. Sci.* 69, 185–194.
- 775 Maupin, C.R., Quinn, T.M., 2008. Extracting a climate signal from the skeletal
776 geochemistry of the Caribbean coral *Siderastrea siderea*. *Geochemistry,*
777 *Geophysics, Geosystems* 9, 13.
- 778 Meehl, G. A., C. Covey, T. Delworth, M. Latif, B. McAvaney, J. F. B. Mitchell, R. J.
779 Stouffer, and K. E. Taylor, 2007b: The WCRP CMIP3 multimodel dataset: A new
780 era in climate change research. *Bull. Amer. Meteor. Soc.*, **88**, 1383–1394.
- 781 Mestas-Nuñez AM, Enfield DB, Zhang C (2007) Water vapor fluxes over the Intra
782 Americas Sea: Seasonal and interannual variability and associations with rainfall.
783 *J Clim* 20: 1910-1922.
- 784 Meinen, C.S., Baringer, M.O. & Garcia, R.F., 2010. Florida Current transport
785 variability: An analysis of annual and longer-period signals. *Deep Sea Research*
786 *Part I: Oceanographic Research Papers*, 57(7), pp.835–846.
- 787 Mignot., et al., Control of Salinity on the mixed layer depth in the world ocean. Part 2,
788 *Journal of Geophysical Research*, 112, 2007.
- 789 Minder J. R., R. B. Smith, and A. D. Nugent, 2013: The Dynamics of Ascent-Forced
790 Orographic Convection in the Tropics: Results from Dominica*. *J. Atmos. Sci.*,
791 70, 4067–4088.
- 792 Misra, V., S. Chan, R. Wu, and E. Chassignet, 2009: Air-sea interaction over the
793 Atlantic warm pool in the NCEP CFS. *Geophys. Res. Lett.*, 36, L15702,
794 doi:10.1029/2009GL038737.
- 795 Misra, V. , A. Stroman, and S. DiNapoli, 2013: The rendition of the Atlantic warm pool
796 in the reanalyses *Clim. Dyn.*, 41, 517-532, doi:10.1007/s00382-012-1474-1.
- 797 Misra, V. and S. DiNapoli, 2013: The observed teleconnection between the equatorial
798 Amazon and the Intra-Americas Seas *Clim. Dyn.*, 40(11-12), 2637-2649,
799 doi:10.1007/s00382-012-1474-1.

- 800 Misra, V., H. Li, and M. Kozar, 2014: The precursors in the Intra-Americas Seas to
801 seasonal climate variations over North America *J. Geophys. Res. (Oceans)*,
802 119(5), 2938-2948, doi:10.1002/2014JC009911.
- 803 Misra, V. and H. Li, 2014: The seasonal climate predictability of the Atlantic Warm
804 Pool and its Teleconnections *Geophys. Res. Lett.*, 41(2), 661-666,
805 doi:10.1002/2013GL058740.
- 806 Misra, V., H. Li, S. Brenner, B. Nag, and A. Mishra, 2015: The sensitivity of the
807 regional coupled ocean-atmosphere downscaling of global reanalysis over the
808 Intra-Americas Seas to the prescribed bathymetry. *Ocean Modeling*. Submitted.
- 809 Molinari, J., D. Knight, M. Dickinson, D. Vollaro, S. Skubis, 1997: Potential Vorticity,
810 Easterly Waves, and Eastern Pacific Tropical Cyclogenesis. *Mon. Wea. Rev.*,
811 125, 2699–2708.
- 812 Muñoz E., A. J. Busalacchi, S. Nigam and A. Ruiz-Barradas, 2008: Winter and summer
813 structure of the Caribbean low-level jet. *J. Climate*, 21, 1260-1276.
- 814 Muñoz, E., and D. Enfield, 2011: The boreal spring variability of the Intra-Americas
815 low-level jet and its relation with precipitation and tornadoes in the eastern United
816 States. *Climate Dyn.*, 36, 247–259, doi:10.1007/s00382-009-0688-3.
- 817 Neelin, J. D., M. Münnich, H. Su, J. E. Meyerson, and C. E. Holloway, 2006: Tropical
818 drying trends in global warming models and observations. *Proc. Natl. Acad. Sci.*
819 USA, **103**, 6110–6115.
- 820 Pailler, et al., The barrier layer in the western tropical Atlantic Ocean. *Geophysical*
821 *Research Letters*, 26(14), 1999.
- 822 Patricola, C.M., R. Saravanan and P. Chang, 2014: The Impact of the El Nio-Southern
823 Oscillation and Atlantic Meridional Mode on Seasonal Atlantic Tropical Cyclone
824 Activity, *J. Clim* , 27 , 5311-5328. doi: [http://dx.doi.org/10.1175/JCLI-D-13-](http://dx.doi.org/10.1175/JCLI-D-13-00687.1)
825 00687.1.
- 826 Poveda, G., and Mesa, O. On the existence of Lloró (the rainiest locality on Earth):
827 Enhanced ocean-land-atmosphere interaction by a low-level jet. *Geophys. Res.*
828 *Lett.* 27 (2000), 1675–1678.
- 829 Poveda G., and O. J. Mesa (1997), Feedbacks between hydrological processes in
830 tropical South America and large-scale ocean-atmospheric phenomena, *J.*
831 *Climate*, Vol. 10, No. 10, 2690-2702.
- 832 Poveda, G., and O. J. Mesa, 1999: The westerly Colombian low-level jet (“CHOCO”)
833 and two other low-level jets over Colombia: Climatology and variability during
834 ENSO phases (In Spanish), *Revista Academia Colombiana de Ciencias, Exactas,*
835 *Físicas y Naturales*, Vol. 23, No. 89, 517-528.

- 836 Poveda, G., et al. (2006), Annual and inter-annual variability of the present climate in
837 northern South America and southern Mesoamerica, *Palaeo-geogr.*
838 *Palaeoclimatol. Palaeoecol.*, 234, 3–27.
- 839 Poveda, G., D. M. Álvarez, and O. A. Rueda (2011), Hydro-climatic variability over
840 the Andes of Colombia associated with ENSO: a review of climatic processes and
841 their impact on one of the Earth's most important biodiversity hotspots, *Climate*
842 *Dynamics*, 36 (11-12), 2233-2249; DOI: 10.1007/s00382-010-0931-y.
- 843 Poveda, G., L. Jaramillo, and L. F. Vallejo, 2014: Seasonal precipitation patterns along
844 pathways of South American low-level jets and aerial rivers, *Water Resour. Res.*,
845 50, 98–118, doi:10.1002/2013WR014087.
- 846 Rauscher, S. A., F. Kucharski, and D. B. Enfield, 2011: The Role of Regional SST
847 Warming Variations in the Drying of Meso-America in Future Climate
848 Projections*. *J. Climate*, **24**, 2003–2016.
- 849 Rayner, N. A., D. E. Parker, E. B. Horton, C. K. Folland, L. V. Alexander, D. P.
850 Rowell, E. C. Kent, and A. Kaplan, 2003: Global analyses of sea surface
851 temperature, sea ice, and night marine air temperature since the late nineteenth
852 century. *J. Geophys. Res.*, **108**, 4407.
- 853 Reynolds RW, Smith TM, Liu C, Chelton DB, Casey KS, Schlat MG (2007) Daily
854 high-resolution blended analyses for sea surface temperature. *J Clim* 20:5473–
855 5496.
- 856 Richter, I., and S.-P. Xie, 2008: On the origin of equatorial Atlantic biases in coupled
857 general circulation models. *Climate Dynamics*, 31, 587-598.
- 858 Richter, I. and coauthors, 2014: Equatorial Atlantic variability and its relation to mean
859 state biases in CMIP5. *Clim. Dyn.*, 42, 171-188.
- 860 Richey, J.N., Poore, R.Z., Flower, B.P., Quinn, T.M., 2007. 1400 yr multiproxy record
861 of climate variability from the northern Gulf of Mexico. *Geology* 2007, 4.
- 862 Richey, J.N., Poore, R.Z., Flower, B.P., Quinn, T.M., Hollander, D.J., 2009. Regionally
863 coherent Little Ice Age cooling in the Atlantic Warm Pool. *Geophysical Research*
864 *Letters* 36, 5.
- 865 Rosenheim, B.E., Swart, P.K., Thorrold, S.R., Eisenhauer, A., Willenz, P., 2005.
866 Salinity change in the subtropical Atlantic: Secular increase and teleconnections
867 to the North Atlantic Oscillation. *Geophysical Research Letters* 32.
- 868 Rousset, C. & Beal, L.M., 2014. Closing the transport budget of the Florida Straits.
869 *Geophysical research letters*, 41(7), pp.2014GL059498–n/a.
- 870 Ruiz-Barradas, A. and S. Nigam, 2005: Warm season rainfall variability over the US
871 great plains in observations, NCEP and ERA-40 Reanalyses, and NCAR and
872 NASA Atmospheric Model Simulations, *J. Climate*, 18, 1808-1830.

- 873 Ruiz-Barradas, A. and S. Nigam, 2006: Great Plains hydroclimate variability: The view
874 from North American Regional Reanalysis. *J. Climate*, 19, 3004-3010.
- 875 Rydbeck, A. V., E. D. Maloney, S.-P. Xie, J. Hafner, and J. Shaman, 2013: Remote
876 forcing versus local feedback of east Pacific intraseasonal variability. *J. Climate*,
877 26, 3575–3596.
- 878 Rydbeck, A. V., and E. D. Maloney, 2014: Energetics of east Pacific easterly waves
879 during intraseasonal events. *J. Climate*, 27, 7603-7621.
- 880 Schmitz, J. T., and S. L. Mullen, 1996: Water Vapor Transport Associated with the
881 Summertime North American Monsoon as Depicted by ECMWF Analyses.
882 *Journal of Climate*, 9, 1621–1634, doi:10.1175/1520-
883 0442(1996)009<1621:WVTAWT>2.0.CO;2
- 884 Schubert, S., D. Gutzler, H. L. Wang, A. Dai, T. Delworth, C. Deser, K. Findell, R. Fu,
885 W. Higgins, M. Hoerling, B. Kirtman, R. Koster, A. Kumar, D. Legler, D.
886 Lettenmaier, B. Lyon, V. Magana, K. Mo, S. Nigam, P. Pegion, A. Phillips, R.
887 Pulwarty, D. Rind, A. Ruiz–Barradas, J. Schemm, R. Seager, R. Stewart, M.
888 Suarez, J. Syktus, M. F. Ting, C. Z. Wang, S. Weaver and N. Zeng, 2009: A US
889 CLIVAR Project to Assess and Compare the Responses of Global Climate
890 Models to Drought–Related SST Forcing Patterns: Overview and Results. *J.*
891 *Climate*, 22(19): 5251–5272.
- 892 Smith, T. M., and R. W. Reynolds, T. C. Peterson, and J. Lawrimore, 2008:
893 Improvements to NOAA’s historical merged land–ocean surface temperature
894 analysis (1880–2006). *J. Climate*, 21, 2283–2296.
- 895 Schumann, S. A., J. Moser, G. A. Johnson, N. D. Walker, and S. A. Hsu, 1995: An
896 overview of a strong winter low in the Gulf of Mexico 12-13 March 1993,
897 *National Weather Digest*, 20 (1). Available from
898 [http://www.nwas.org/digest/papers/1995/Vol20-Issue1-Oct1995/Pg11-](http://www.nwas.org/digest/papers/1995/Vol20-Issue1-Oct1995/Pg11-Schumann.pdf)
899 [Schumann.pdf](http://www.nwas.org/digest/papers/1995/Vol20-Issue1-Oct1995/Pg11-Schumann.pdf)
- 900 Serra, Y. L., G. N. Kiladis, and M. F. Cronin, 2008: Horizontal and vertical structure of
901 easterly waves in the Pacific ITCZ. *J. Atmos. Sci.*, 65, 1266-1284.
- 902 Serra, Y. L., G. Kiladis, and K. Hodges, 2010: Tracking and Mean Structure of Easterly
903 Waves Over the Intra-Americas Sea. *J. Climate*, 23, 4823-4840.
- 904 Serra, Y. L., X. Jiang, B. Tian, J. Amador Astua, E. D. Maloney, and G. N. Kiladis,
905 2014: Tropical intra-seasonal oscillations and synoptic variability. *Annual Review*
906 *of Environment and Resources*, in press.
- 907 Sheffield, J., A. Barrett, B. Colle, R. Fu, K. L. Geil, Q. Hu, J. Kinter, S. Kumar, B.
908 Langenbrunner, K. Lombardo, L. N. Long, E. Maloney, A. Mariotti, J. E.
909 Meyerson, K. C. Mo, J. D. Neelin, Z. Pan, A. Ruiz-Barradas, Y. L. Serra, A. Seth,
910 J. M. Thibeault, J. C. Stroeve, 2013: North American climate in CMIP5

- 911 experiments. Part I: Evaluation of 20th Century continental and regional
912 climatology. *J. Climate*, 26, 9209-9245.
- 913 Sheinbaum, J. et al., 2002. Flow structure and transport in the Yucatan Channel.
914 *Geophysical research letters*, 29(3), pp.10–11.
- 915 Skamarock, W. C., J. B. Klemp, J. Dudhia, D. O. Gill, D. M. Barker, M. G. Duda, X.
916 Huang, W. Wang, and J. G. Powers, A description of the Advanced Research
917 WRF Version 3, NCAR Technical Note, 2008.
- 918 Smith R. B., J. R. Minder, A. D. Nugent, T. Storelvmo, D. J. Kirshbaum, R. Warren, N.
919 Lareau, P. Palany, A. James, and J. French, 2012: Orographic Precipitation in the
920 Tropics: The Dominica Experiment. *Bull. Amer. Meteor. Soc.*, 93, 1567–1579.
- 921 Smith, J.M., Quinn, T.M., Helmle, K.P., Halley, R.B., 2006. Reproducibility of
922 geochemical and climatic signals in the Atlantic coral *Montastraea faveolata*.
923 *Paleoceanography* 21, doi:10.1029/2005PA001187.
- 924 Sobel, A., Burleyson, C., and Yuter, S., 2011: Rain on small tropical islands. *J.*
925 *Geophys. Res.*, 116, D08102, doi:10.1029/2010JD014695.
- 926 Sprintall, J. and M. Tomczak, 1992:Evidence of the barrier layer in the surface layer of
927 the tropics, *Journal of Geophysical Research*, 97 (C5), 7305–7316.
- 928 Taylor, K. E., R. J. Stouffer, and G. A. Meehl, 2012: An overview of CMIP5 and the
929 experiment design. *Bull. Amer. Meteor. Soc.*, **93**, 485–498.
- 930 Ting, M., Y. Kushnir, R. Seager and L. Cuihua, 2011: Robust features of Atlantic
931 multi-decadal variability and its climate impacts. *Geophys. Res. Lett.*, **38**, L17705.
- 932 Ting, M. F., Y. Kushnir, R. Seager and C. H. Li, 2009: Forced and Internal Twentieth–
933 Century SST Trends in the North Atlantic. *J. Climate*, **22**(6): 1469–1481.
- 934 Toma, V. E., and P. J. Webster, 2010a: Oscillations of the intertropical convergence
935 zone and the genesis of easterly waves. Part I: diagnostics and theory. *Climate*
936 *Dyn.*, 34, 587-604.
- 937 Toma, V. E., and P. J. Webster, 2010b: Oscillations of the Intertropical Convergence
938 Zone and the genesis of easterly waves Part II: numerical verification. *Climate*
939 *Dyn.*, 34, 605-613.
- 940 Tuluy, H. A., G. M. Grandolini, E. J. Ijjasz-Vasquez, K. E. Kemper, and J. Zuleta,
941 2012: Project Appraisal Document on a Proposed Loan in the Amount of
942 US\$105,263,157.89 to the United Mexican States for the Modernization of the
943 National Meteorological Service for Improved Climate Adaptation Project. World
944 Bank, 1 pp.

- 945 Vimont, D. J., and J. P. Kossin, 2007: The Atlantic meridional mode and hurricane
946 activity. *Geophys. Res. Lett.*, 34, L07709, doi:10.1029/2007GL029683.
- 947 Vizzy, E. and K. Cook, 2010: Influence of the Amazon/Orinoco Plume on the
948 summertime Atlantic climate. *Journal of Geophysical Research*, 115 (D21), D21
949 112.
- 950 Wang, C., and D. B. Enfield, 2001: The tropical western hemisphere warm pool.
951 *Geophys. Res. Lett.*, 28, 1635-1638.
- 952 _____, and D. B. Enfield. A further study of the tropical Western Hemisphere Warm
953 Pool. *J. Climate*, 6, 1476-1493 (2003).
- 954 _____, D. B. Enfield, S. -K. Lee, and C. Landsea. Influences of the Atlantic warm pool
955 on Western Hemisphere summer rainfall and Atlantic hurricanes. *J. Climate*, 19,
956 3011-3028 (2006).
- 957 _____, 2007: Variability of the Caribbean low-level jet and its relations to climate.
958 *Clim. Dyn.*, 29:411-422.
- 959 _____, and S. -K. Lee. Atlantic warm pool, Caribbean low-level jet, and their potential
960 impact on Atlantic hurricanes. *Geophys. Res. Lett.*, 34, (2007).
- 961 _____, S. -K. Lee, and D. B. Enfield. Climate response to anomalously large and small
962 Atlantic Warm pools during the summer. *J. Climate*, 21, 2437-2450 (2008a).
- 963 Wang, C., S.-K. Lee, and C. R. Mechoso, 2010: Interhemispheric influence of the
964 Atlantic warm pool on the Southeastern Pacific. *Journal of Climate*, 23:404-418.
- 965 Wang, C., H. Liu, S.-K. Lee, and R. Atlas, 2011: Impact of the Atlantic warm pool on
966 United States landfalling hurricanes. *Geophysical Research Letters*, 38, L19702,
967 doi:10.1029/2011GL049265.
- 968 Wang, C., and L. Zhang, 2013: Multidecadal ocean temperature and salinity variability
969 in the tropical North Atlantic: Linking with the AMO, AMOC and subtropical
970 cell. *Journal of Climate*, 26, 6137-6162.
- 971 Wang, C., L. Zhang, S.-K. Lee., L. Wu, and C. R. Mechoso, 2014: A global perspective
972 on CMIP5 climate model biases. *Nature Climate Change* , 4 , 201-205.
- 973 Wang, H., and R. Fu, 2002: Cross-equatorial flow and seasonal cycle of precipitation
974 over South America. *J. Clim.*, 15, 1591–1608.
- 975 Waylen, P. R., et al. (1996), Temporal and spatial variability of annual precipitation in
976 Costa Rica and the Southern Oscillation, *Int. J. Climatol.*, 16, 173–193
- 977 Weisberg, R. H. On the evolution of SST over the PACS region, Abstracts of 76 'h
978 AMS Annual Meeting, Atlanta, Georgia, Amer. Meteor. Soc., 378 (1996).

979 Xie, S.-P., 1996: Westward propagation of latitudinal asymmetry in a coupled ocean-
980 atmosphere model. *J. Atmos. Sci.*, 53, 3236–3250.

981 Xu, Z., P. Chang, I. Richter and W.-M. Kim, 2014: Diagnosing Southeast Tropical
982 Atlantic SST and Ocean Circulation Biases in the CMIP5 Ensemble, *Clim. Dyn.* ,
983 DOI10.1007/s00382-014-2247-9.

984 Zhang, L., and C. Wang, 2012: Remote influences on freshwater flux variability in the
985 Atlantic warm pool region. *Geophysical Research Letters*, 39, L19714,
986 doi:10.1029/2012GL053530.

987 Zhang L., C. Wang and S.-K. Lee , 2014: Potential role of Atlantic warm pool-induced
988 freshwater forcing in the Atlantic meridional overturning circulation: Ocean-sea
989 ice coupled model simulations. *Climate Dynam.*, doi:10.1007/s00382-013-2034-
990 z., in-press .

991

992 **Figure Captions**

993 Figure 1: a) The mean June-July-August-September (JJAS) climatological SST
994 (Reynolds et al. 2007; contoured) with the 28.5°C isotherm (marking the boundary of
995 the WHWP) in bold black line with mean climatological JJAS 925hPa winds (from
996 Climate Forecast System Reanalysis [Saha et al. 2010]), and mean climatological JJAS
997 mean rainfall (from Chen et al. 2002; shaded). b) The orography of the Americas and
998 the bathymetry of the neighboring oceans.

999 Figure 2: Summertime (JJA) atmospheric teleconnections linked to large minus small
1000 AWP in (top panels) observations, (middle panel) AGCM and (bottom panels) simple
1001 model experiments (see Lee et al. 2009). Left panels show baroclinic stream function
1002 and rotational wind anomalies (750 minus 250hPa and divided by 2) and the right
1003 panels show barotropic streamfunction and rotational wind anomalies (750 plus 250mb
1004 divided by 2). The observations are based on ERSST3 and NCEP reanalysis, the
1005 AGCM results are from Wang et al. (2008), and the simple model results are from Lee
1006 et al. (2009). The unit for stream function is $10^{-6} \text{ m}^2 \text{ s}^{-1}$.

1007 Figure 3: The correlation of the June-October AWP area anomalies (SST from
1008 Reynolds et al. 2007) with corresponding a) rainfall anomalies (shaded; rainfall from
1009 Chen et al. 2002) and b) mean sea level pressure (MSLP) anomalies (shaded; MSLP
1010 from Saha et al. 2010) and regression of June-September AWP area anomalies on
1011 corresponding 925hPa wind anomalies (winds from Saha et al. 2010). The significant
1012 values at 95% confidence interval according to t-test are contoured and vectors are
1013 shown in red.

1014 Figure 4: Linear trend in SST from “super ensemble” consisting of HadlSST1,
1015 KaplanSST2, ERSST3b and COBE2 reanalysis of the iCOADS data set. Masked
1016 (white) areas are where the sign of the trend in all 4 analysis products does not match;
1017 colored areas are average trends where all four products match in sign. Circles show
1018 sites where proxy reconstructions have positive (red) centennial trends or insignificant
1019 (white) trends. Magnitudes of proxy trends are generally higher than the observational
1020 data set. Boxes indicate areas for which Caribbean and Gulf of Mexico time series are
1021 calculated (see SM S.1).

1022 Figure 5: The correlation of the June-July-August mean SST anomalies (OISST) with
1023 preceding December-February rainfall anomalies (CRU) over equatorial Amazon
1024 (outlined). These correlations are computed over 1995-2004 period after the linear
1025 trends in rainfall and SST are removed and only significant values at 90% confidence
1026 interval are shown. Adapted from Misra and DiNapoli (2013).

1027 Figure 6: Climatological annual mean rainfall (mm/day) computed between 1998 and
1028 2013 from TRMM 3B43 (0.25° resolution) and GPCP 1-degree daily (1DD) data (1°
1029 resolution) for four regions in the IAS: a) Caribbean wide (10-25°N, 60-90°W), b)
1030 Central America (8-22°N, 83-95°W), c) the Greater Antilles (16-24°N, 65-87°W), and
1031 d) the Lesser Antilles (11-20°N, 58-65°W).

1032

1033 Figure 7: Mean climatological SST (°C) in the Caribbean Sea for January-February-
1034 March (a) January-February-March, (b) April-May-June, (c) July-August-September, and
1035 (d) November-December-October from NOAA Ocean Watch blended SST product
1036 (<http://oceanwatch.pfeg.noaa.gov/thredds/Satellite/aggregsatBA/ssta/catalog.html>). The

1037 mean is constructed over a period of 2003–2014.

1038

1039 Figure 8: The composite of Atlantic tropical cyclone track density (per $3^\circ \times 3^\circ$ cell) for
1040 a) 10 largest AWP years (2010, 2005, 1998, 2012, 2011, 2006, 2003, 1987, 2004, 2008)
1041 and b) 10 smallest AWP years
1042 (1984, 1986, 1982, 1985, 1994, 1992, 1989, 1993, 1996, 1991), selected between 1979–2012.

1043 There were 163 and 90 named tropical cyclones in the 10 selected largest and smallest
1044 AWP years respectively.

1045

1046 Figure 9. Incidents of intense (F3–F5) U.S. tornadoes in April–May for (a) the top 10
1047 most active years, (b) 10 least active years during 1950–2010 obtained from Severe
1048 Weather database. Green indicates F3, blue F4, and red F5 tornadoes. Anomalous
1049 moisture transport for the (c) 10 most active and (d) 10 least active U.S. tornado years
1050 in April–May during 1950–2010 obtained from NCEP reanalysis. The unit for moisture
1051 transport is $\text{kg m}^{-1}\text{s}^{-1}$. The small boxes in (c) and (d) indicate the central and eastern
1052 U.S. region frequently affected by intense tornadoes ($30\text{--}40\text{N}$, $100\text{--}80\text{W}$). This figure
1053 is reproduced from Lee et al. (2013).

1054

1055 Figure 10: SST (contoured in $^\circ\text{C}$; from Reynolds et al. 2007), Sea Surface Height
1056 anomalies (shaded in m; from <http://aviso.oceanobs.com>) and track of observed
1057 minimum sea level pressure of the March 9–13 Superstorm of 1993.

1058 Figure 11: The average monthly Atlantic Warm pool areas (in $\times 10^6 \text{ km}^2$) from 1909–
1059 2005 based on various CMIP5 20th century simulations and ERSSTv3 observations.

1060 Each cell in the table is color coded (cool colors indicate a small AWP; warm colors
1061 indicate a large AWP) in order to show the average seasonal evolution of the Atlantic
1062 Warm Pool's areal extent. Adapted from Kozar and Misra (2012).

1063

1064 Figure 12: Annual mean SST biases in CMIP5 (a) and CMIP3 (b) model ensembles.

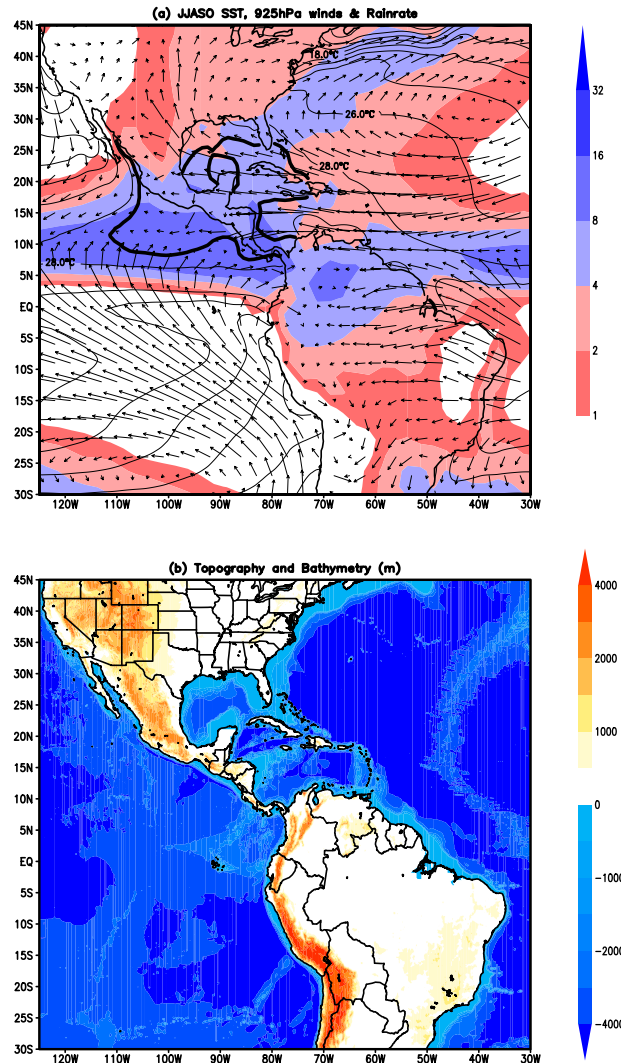
1065 The biases are referenced to observed Reynolds SST. After Xu et al. 2014.

1066

1067 Fig. 13: Anomaly correlation (AC) skill of SST prediction for seasonal means of June-
1068 July-August (JJA). AC is computed based on the NMME hindcasts over the 1981-2010
1069 period. The NMME ensemble initialized in March was used.

1070 Figure 14: Same as Fig. 13 but for seasonal mean June-July-August (JJA) precipitation
1071 anomaly.

1072

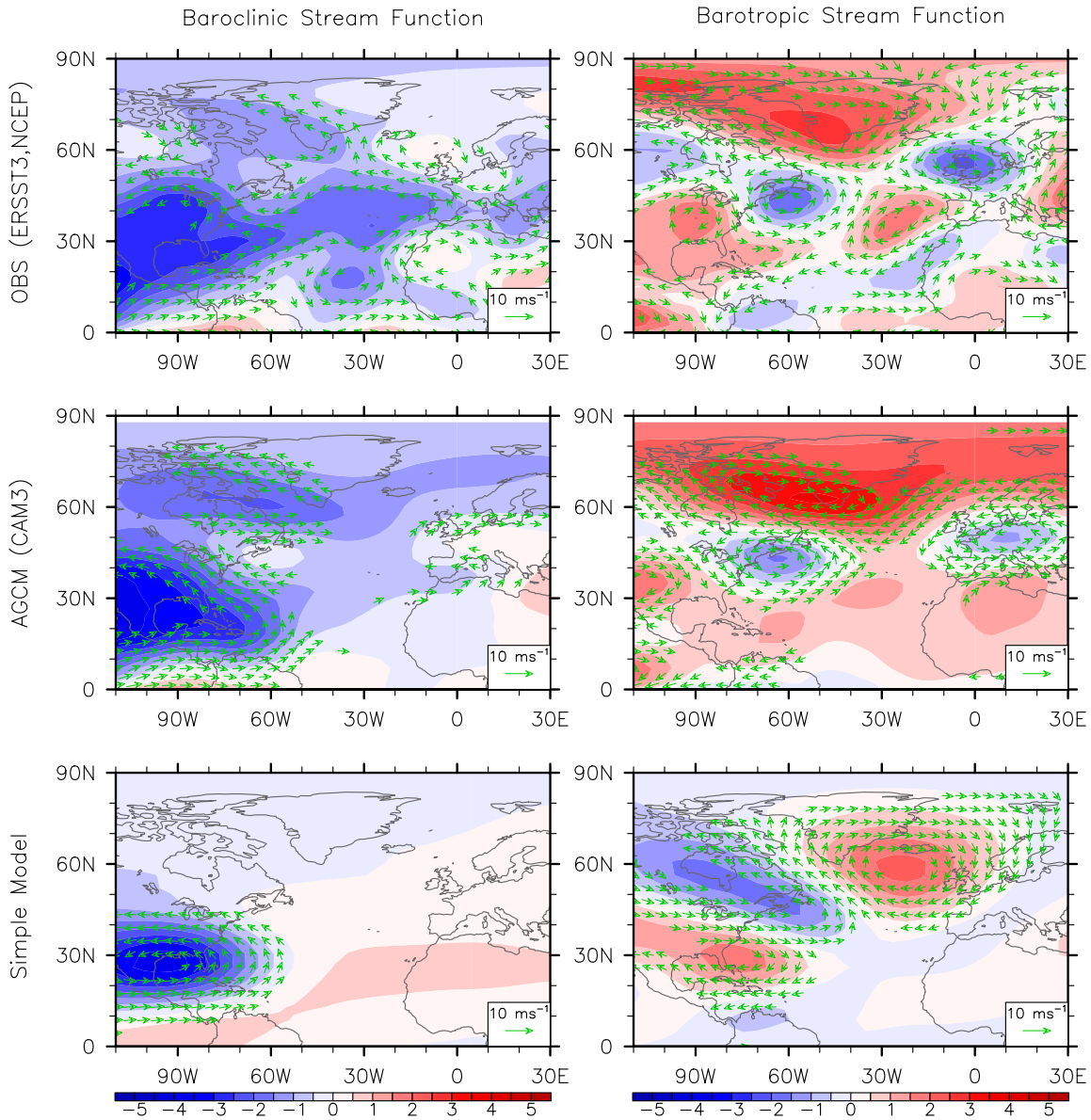


→
10

1073

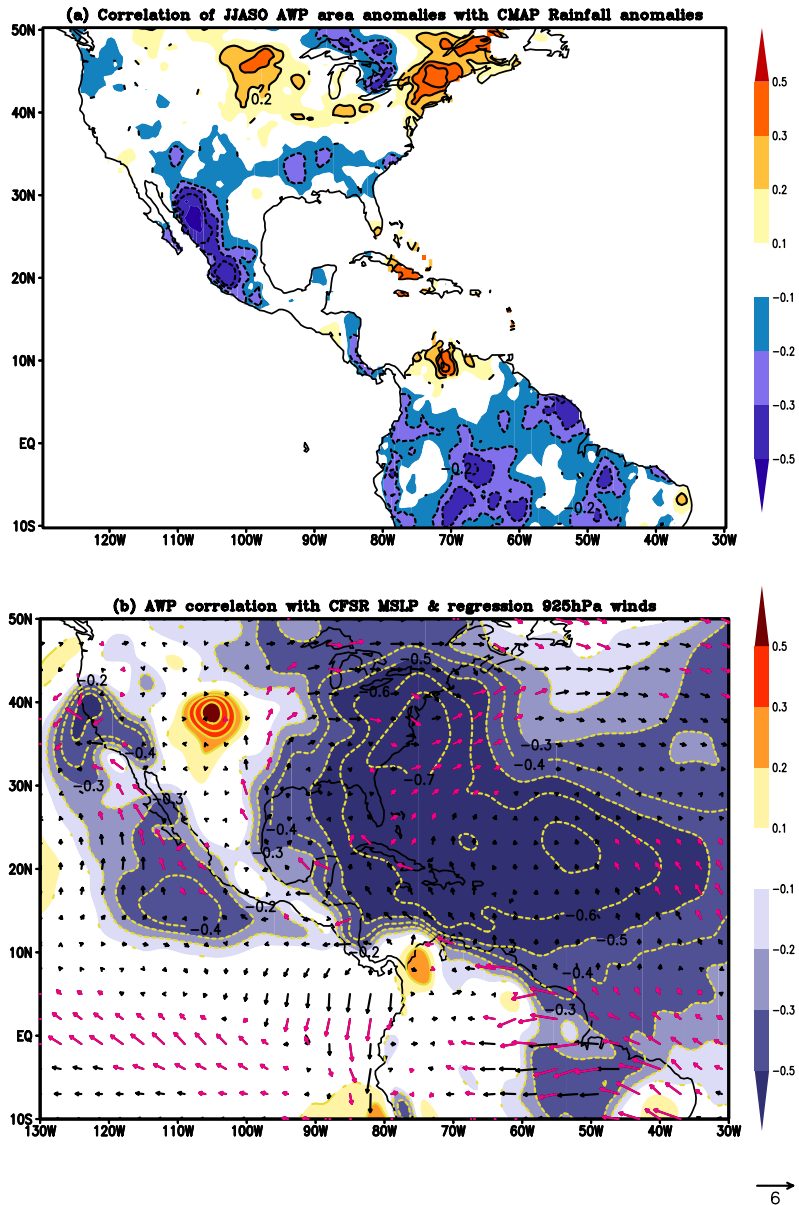
1074 Figure 1: a) The mean June-July-August-September-October (JJASO) climatological SST
 1075 (Reynolds et al. 2007; contoured) with the 28.5°C isotherm (marking the boundary of the
 1076 WHWP) in bold black line with mean climatological JJASO 925hPa winds (from Climate
 1077 Forecast System Reanalysis [Saha et al. 2010]), and mean climatological JJASO mean
 1078 rainfall (from Chen et al. 2002; shaded). b) The orography of the Americas and the
 1079 bathymetry of the neighboring oceans.

Summertime Atmospheric Teleconnections Linked to Large–Small AWP



1080

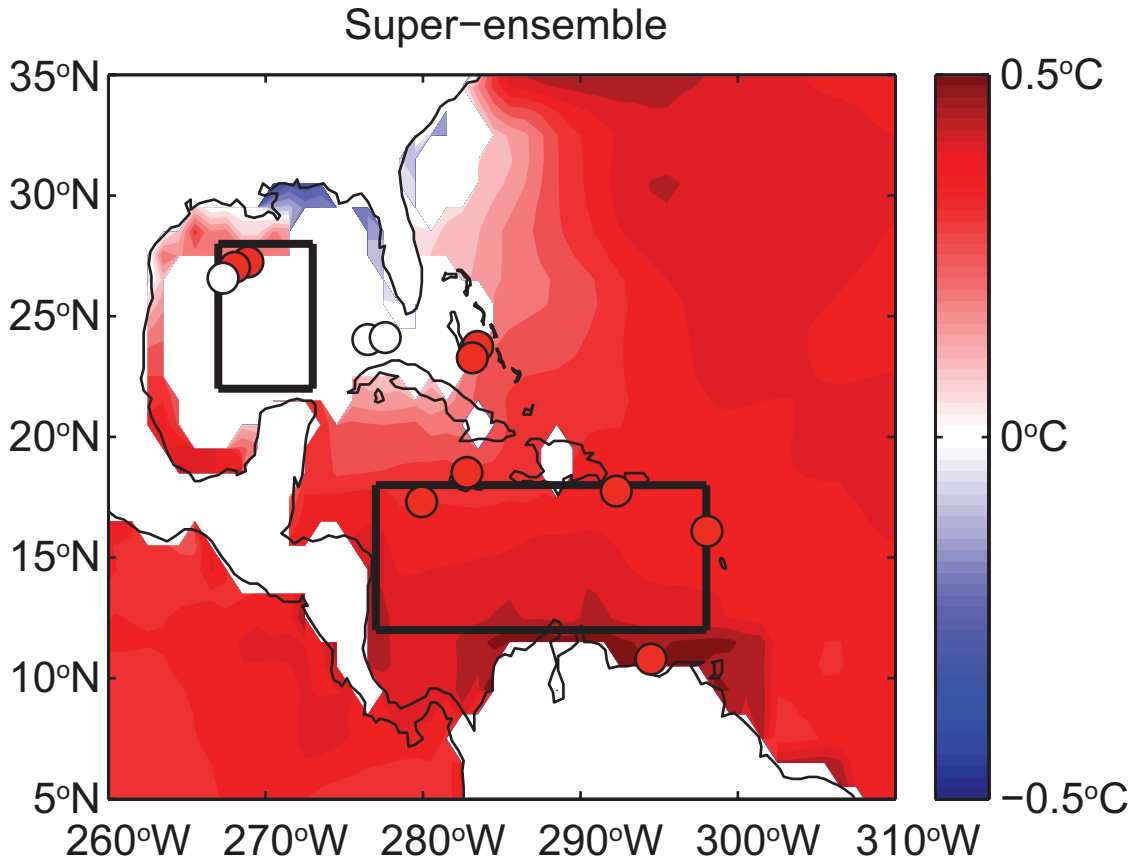
1081 Figure 2: Summertime (JJA) atmospheric teleconnections linked to large minus small
 1082 AWP in (top panels) observations, (middle panel) AGCM and (bottom panels) simple
 1083 model experiments (see Lee et al. 2009). Left panels show baroclinic steam function and
 1084 rotational wind anomalies (750 minus 250hPa and divided by 2) and the right panels
 1085 show barotropic streamfunction and rotational wind anomalies (750 plus 250mb divided
 1086 by 2). The observations are based on ERSST3 and NCEP reanalysis, the AGCM results
 1087 are from Wang et al. (2008), and the simple model results are from Lee et al. (2009). The
 1088 unit for stream function is $10^{-6} \text{ m}^2 \text{ s}^{-1}$.
 1089



→
6

1090
1091
1092
1093
1094
1095
1096
1097

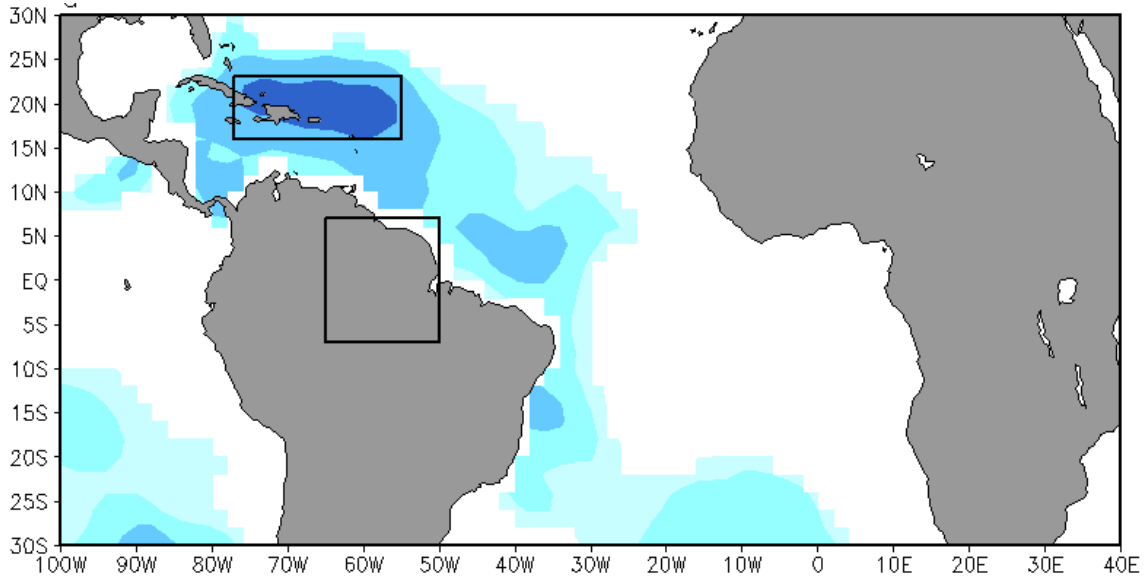
Figure 3: The correlation of the June-October AWP area anomalies (SST from Reynolds et al. 2007) with corresponding a) rainfall anomalies (shaded; rainfall from Chen et al. 2002) and b) mean sea level pressure (MSLP) anomalies (shaded; MSLP from Saha et al. 2010) and regression of June-September AWP area anomalies on corresponding 925hPa wind anomalies (winds from Saha et al. 2010). The significant values at 95% confidence interval according to t-test are contoured and vectors are shown in red.



1098
 1099 Figure 4: Linear trend in SST from “super ensemble” consisting of HadISST1,
 1100 KaplanSST2, ERSST3b and COBE2 reanalysis of the iCOADS data set. Masked (white)
 1101 areas are where the sign of the trend in all 4 analysis products does not match; colored
 1102 areas are average trends where all four products match in sign. Circles show sites where
 1103 proxy reconstructions have positive (red) centennial trends or insignificant (white)
 1104 trends. Magnitudes of proxy trends are generally higher than the observational data
 1105 set. Boxes indicate areas for which Caribbean and Gulf of Mexico time series are
 1106 calculated (see SM S.1).

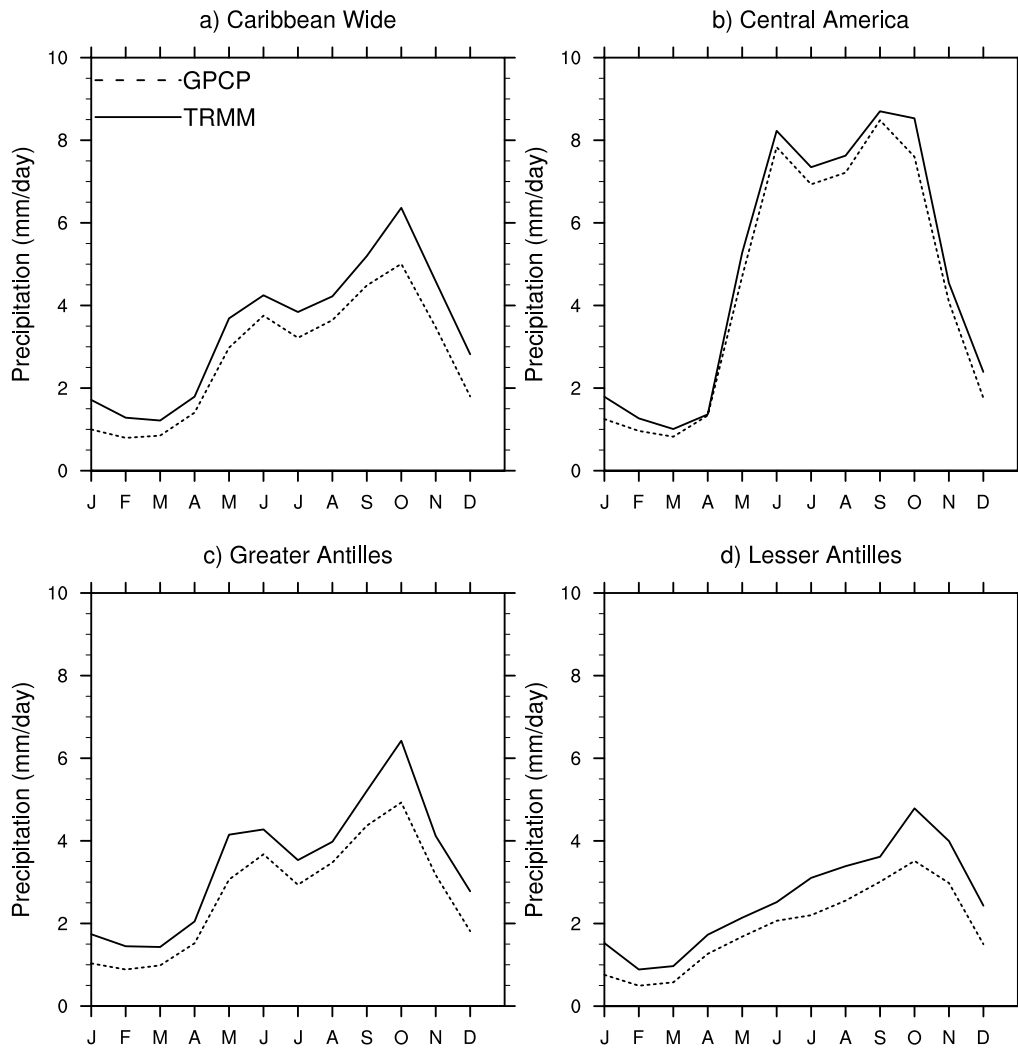
1107

1108

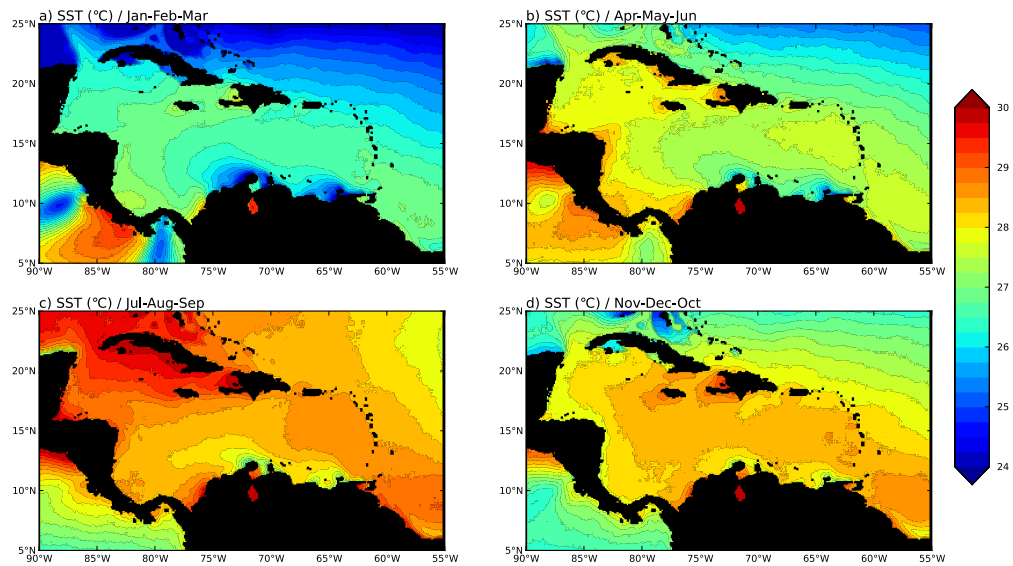


1109

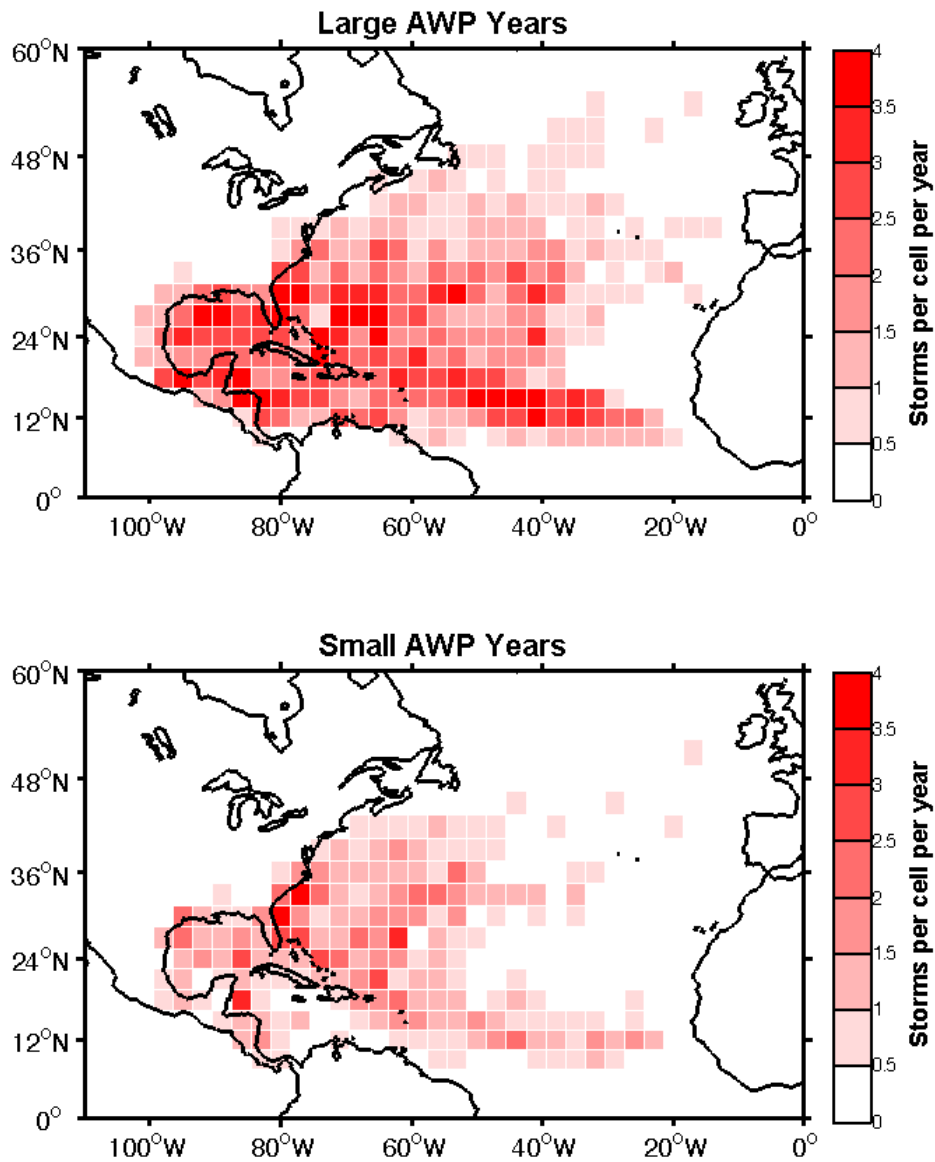
1110 Figure 5: The correlation of the June-July-August mean SST anomalies (OISST) with
1111 preceding December-February rainfall anomalies (CRU) over equatorial Amazon
1112 (outlined). These correlations are computed over 1995-2004 period after the linear trends
1113 in rainfall and SST are removed and only significant values at 90% confidence interval
1114 are shown. Adapted from Misra and DiNapoli (2013).



1115
 1116 Figure 6: Climatological annual mean rainfall (mm/day) computed between 1998 and
 1117 2013 from TRMM 3B43 (0.25° resolution) and GPCP 1-degree daily (1DD) data (1°
 1118 resolution) for four regions in the IAS: a) Caribbean wide (10-25°N, 60-90°W), b)
 1119 Central America (8-22°N, 83-95°W), c) the Greater Antilles (16-24°N, 65-87°W), and d)
 1120 the Lesser Antilles (11-20°N, 58-65°W).
 1121

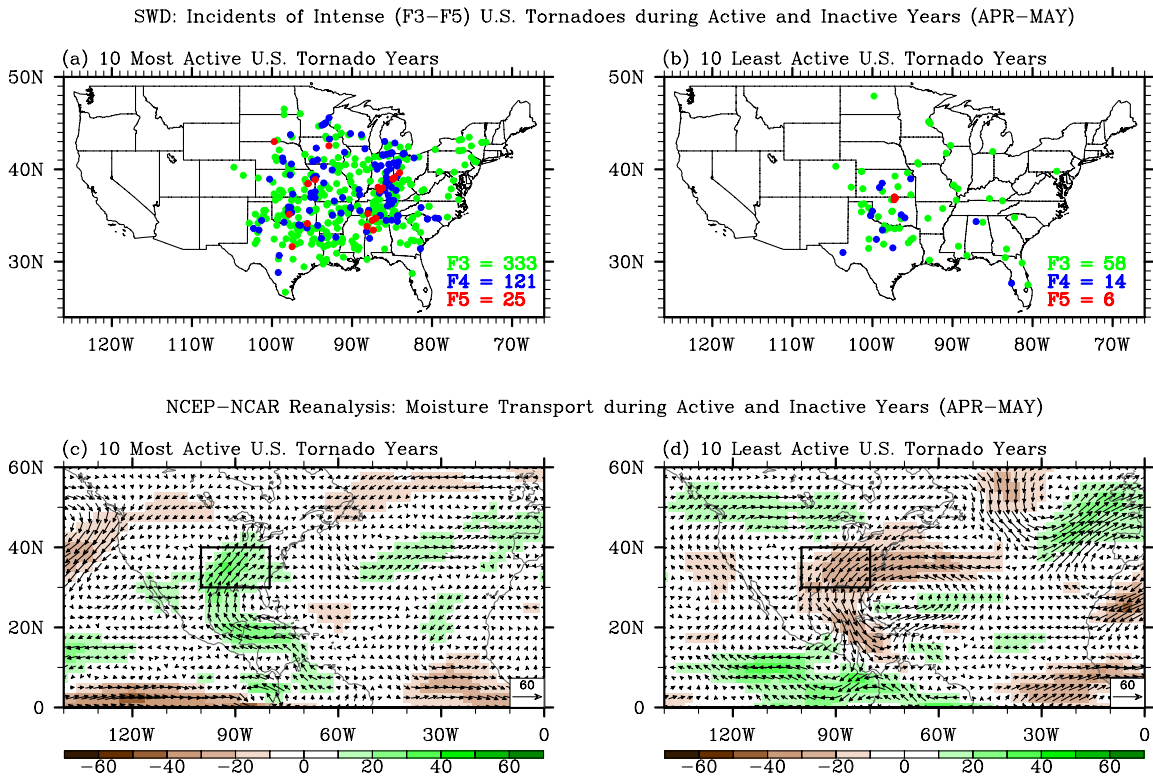


1122
 1123 Figure 7: Mean climatological SST (°C) in the Caribbean Sea for January-February-
 1124 March (a) January-February-March, (b) April-May-June, (c) July-August-September, and
 1125 (d) November-December-October from NOAA Ocean Watch blended SST product
 1126 (<http://oceanwatch.pfeg.noaa.gov/thredds/Satellite/aggregsatBA/ssta/catalog.html>). The
 1127 mean is constructed over a period of 2003–2014.
 1128



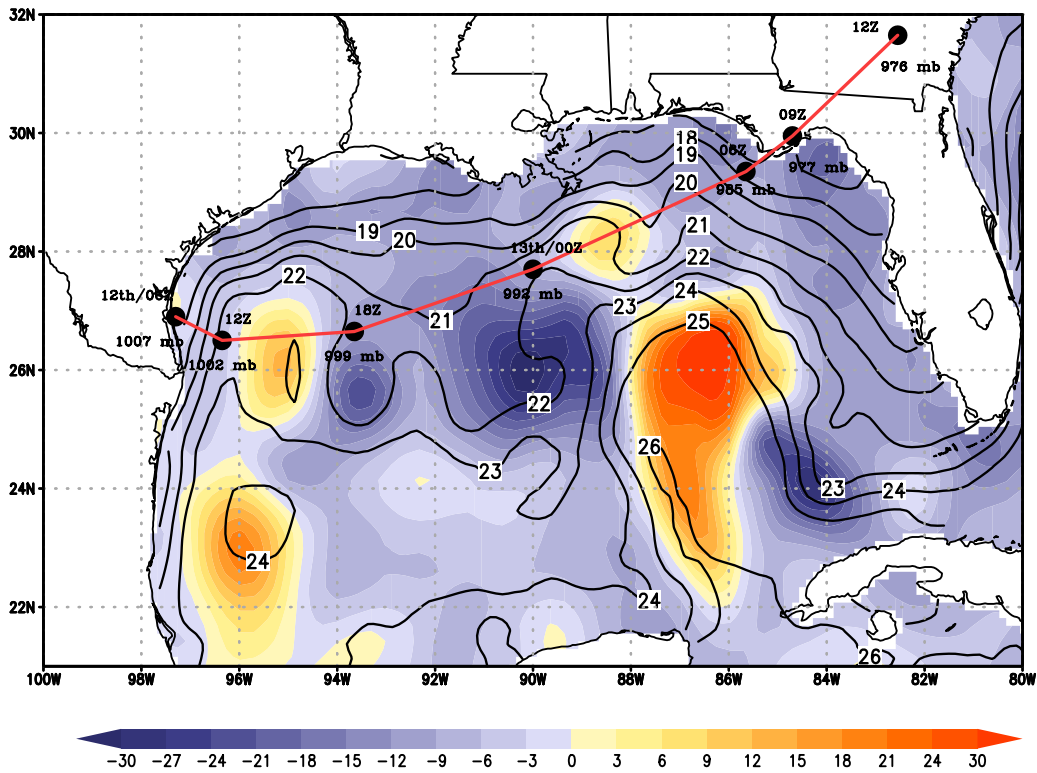
1129
 1130 Figure 8: The composite of Atlantic tropical cyclone track density (per 3°x3 °cell) for a)
 1131 10 largest AWP years (2010, 2005, 1998, 2012, 2011, 2006, 2003, 1987, 2004, 2008) and
 1132 b) 10 smallest AWP years (1984, 1986, 1982, 1985, 1994, 1992, 1989, 1993, 1996, 1991),
 1133 selected between 1979-2012. There were 163 and 90 named tropical cyclones in the 10
 1134 selected largest and smallest AWP years respectively.
 1135

1136
1137
1138



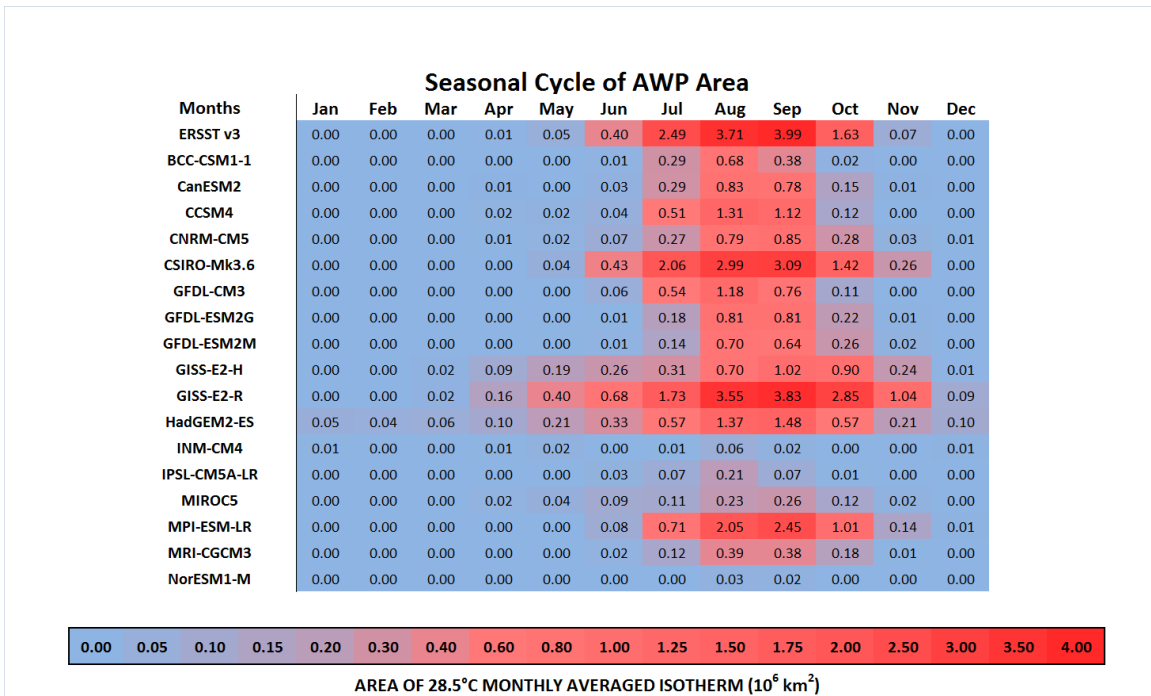
1139
1140
1141
1142
1143
1144
1145
1146
1147
1148

Figure 9. Incidents of intense (F3–F5) U.S. tornadoes in April–May for (a) the top 10 most active years, (b) 10 least active years during 1950–2010 obtained from Severe Weather database. Green indicates F3, blue F4, and red F5 tornadoes. Anomalous moisture transport for the (c) 10 most active and (d) 10 least active U.S. tornado years in April–May during 1950–2010 obtained from NCEP reanalysis. The unit for moisture transport is $\text{kg m}^{-1}\text{s}^{-1}$. The small boxes in (c) and (d) indicate the central and eastern U.S. region frequently affected by intense tornadoes (30–40N, 100–80W). This figure is reproduced from Lee et al. (2013).



1149
 1150 Figure 10: SST (contoured in °C; from Reynolds et al. 2007), Sea Surface Height
 1151 anomalies (shaded in m; from <http://aviso.oceanobs.com>) and track of observed minimum
 1152 sea level pressure of the March 9-13 Superstorm of 1993.

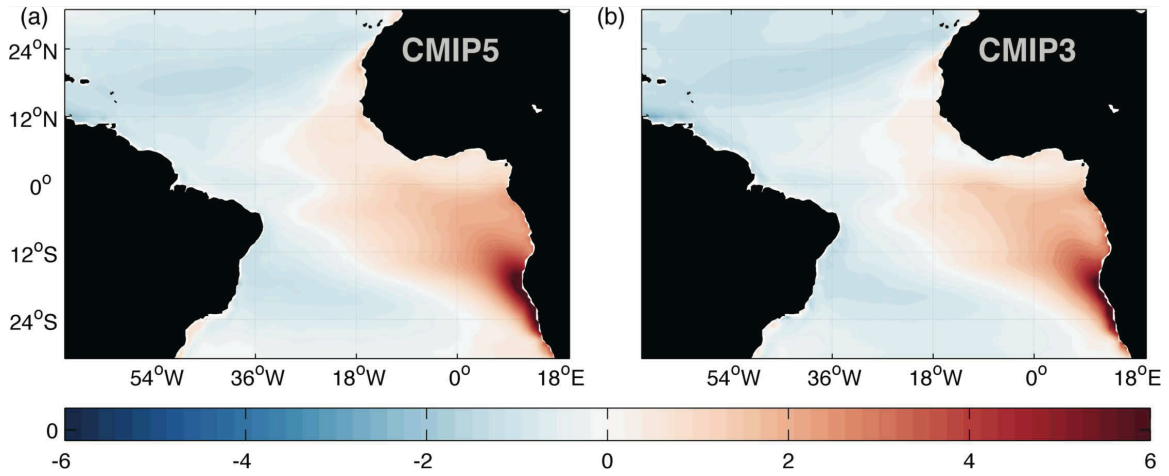
1153



1154

1155 Figure 11: The average monthly Atlantic Warm pool areas (in x10⁶ km²) from 1909–2005
 1156 based on various CMIP5 20th century simulations and ERSSTv3 observations. Each cell
 1157 in the table is color coded (cool colors indicate a small AWP; warm colors indicate a
 1158 large AWP) in order to show the average seasonal evolution of the Atlantic Warm Pool's
 1159 areal extent. Adapted from Kozar and Misra (2012).

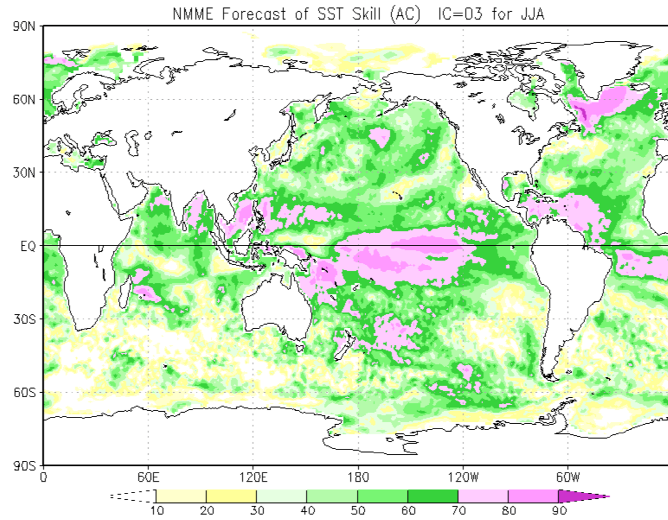
1160



1161

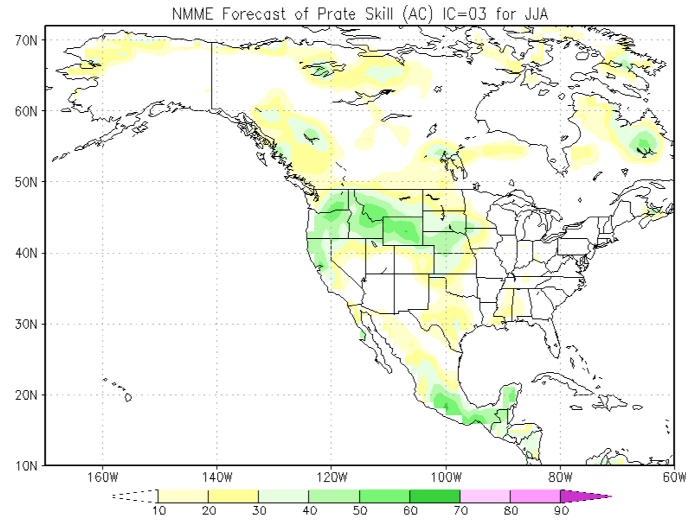
1162 Figure 12: Annual mean SST biases in CMIP5 (a) and CMIP3 (b) model ensembles. The
 1163 biases are referenced to observed Reynolds SST. After Xu et al. 2014.

1164



1165
 1166 Fig. 13: Anomaly correlation (AC) skill of SST prediction for seasonal means of June-
 1167 July-August (JJA). AC is computed based on the NMME hindcasts over the 1981-2010
 1168 period. The NMME ensemble initialized in March was used.

1169



1170

1171 Figure 14: Same as Fig. 13 but for seasonal mean June-July-August (JJA) precipitation
 1172 anomaly.

1173

1174